AFRL-OSR-VA-TR-2015-0092

Influence of Group IV and V Alloying Elements on the Microstructure Engineering

GREGORY THOMPSON
UNIVERSITY OF ALABAMA

04/06/2015
Final Report

Air Force Research Laboratory
AF Office Of Scientific Research (AFOSR)/ RTD
Arlington, Virginia 22203
Air Force Materiel Command

REPORT DOCUMENTATION PAGE

Form Approved
OMB No. 0704-0188

PLEASE DO NOT RETURN YOUR FORM TO THE ABOVE ORGANIZATION.

1. REPORT DATE *(DD-MM-YYYY)*	2. REPORT TYPE	3. DATES COVERED *(From - To)*
28-03-2015	Year 3 and Final Report	01/04/2014 - 31/03/2015

4. TITLE AND SUBTITLE
Influence of Group IV and V Alloying Elements on the Microstructure Engineering and Deformation Behavior in Tantalum Carbides

5a. CONTRACT NUMBER

5b. GRANT NUMBER
FA9550-12-1-0104

5c. PROGRAM ELEMENT NUMBER

6. AUTHOR(S)
Gregory B. Thompson

5d. PROJECT NUMBER

5e. TASK NUMBER

5f. WORK UNIT NUMBER

7. PERFORMING ORGANIZATION NAME(S) AND ADDRESS(ES)
The University of Alabama
Office for Sponsored Programs
301 Rose Administration Building
Tuscaloosa, AL 35487-0104

8. PERFORMING ORGANIZATION REPORT NUMBER

9. SPONSORING/MONITORING AGENCY NAME(S) AND ADDRESS(ES)
Air Force Office of Scientific Research
875 N. Randolph St.
Room 3112
Arlington VA 22203

10. SPONSOR/MONITOR'S ACRONYM(S)
AFOSR

11. SPONSOR/MONITOR'S REPORT NUMBER(S)

12. DISTRIBUTION/AVAILABILITY STATEMENT
Distribution A - Available for Public Release

13. SUPPLEMENTARY NOTES
None

14. ABSTRACT
Tantalum carbides comprise a class of high and ultrahigh melting temperature materials with tremendous thermo-mechanical property potential. This program provided a fundamental series of studies to address how group IVB and VB metal carbide alloying brings about microstructural engineering with subsequent changes in thermo-mechanical behavior. The program employed a combined computational and experimental approach coupled through advanced analytical electron microscopy characterization to address this gap. Major findings include determination of an intrinsic stacking fault on the {111} planes in TaC that circumvents slip on {110}, which is the dominant slip plane in HfC; the competition of vacancy ordered and fault-forming phases with metal-enrichment in Ta-C; the formation of vacancy ordered phase domains which are hypothesized to contribute to an anomalous rise in hardness for the group VB carbides absent in group IVB carbides; and finally construction of a non-contact Lorentz force thermo-mechanically loading apparatus for testing these carbides above 3000 deg. C.

15. SUBJECT TERMS
Tantalum carbides; hafnium carbides; transition metal group IVB carbides; transition metal group VB carbides; TEM; density functional theory; dislocations; phase stability

16. SECURITY CLASSIFICATION OF:			17. LIMITATION OF ABSTRACT	18. NUMBER OF PAGES	19a. NAME OF RESPONSIBLE PERSON
a. REPORT	b. ABSTRACT	c. THIS PAGE			Gregory Thompson
					19b. TELEPHONE NUMBER *(Include area code)* 205-348-1589

Reset

INSTRUCTIONS FOR COMPLETING SF 298

1. REPORT DATE. Full publication date, including day, month, if available. Must cite at least the year and be Year 2000 compliant, e.g. 30-06-1998; xx-06-1998; xx-xx-1998.

2. REPORT TYPE. State the type of report, such as final, technical, interim, memorandum, master's thesis, progress, quarterly, research, special, group study, etc.

3. DATES COVERED. Indicate the time during which the work was performed and the report was written, e.g., Jun 1997 - Jun 1998; 1-10 Jun 1996; May - Nov 1998; Nov 1998.

4. TITLE. Enter title and subtitle with volume number and part number, if applicable. On classified documents, enter the title classification in parentheses.

5a. CONTRACT NUMBER. Enter all contract numbers as they appear in the report, e.g. F33615-86-C-5169.

5b. GRANT NUMBER. Enter all grant numbers as they appear in the report, e.g. AFOSR-82-1234.

5c. PROGRAM ELEMENT NUMBER. Enter all program element numbers as they appear in the report, e.g. 61101A.

5d. PROJECT NUMBER. Enter all project numbers as they appear in the report, e.g. 1F665702D1257; ILIR.

5e. TASK NUMBER. Enter all task numbers as they appear in the report, e.g. 05; RF0330201; T4112.

5f. WORK UNIT NUMBER. Enter all work unit numbers as they appear in the report, e.g. 001; AFAPL30480105.

6. AUTHOR(S). Enter name(s) of person(s) responsible for writing the report, performing the research, or credited with the content of the report. The form of entry is the last name, first name, middle initial, and additional qualifiers separated by commas, e.g. Smith, Richard, J, Jr.

7. PERFORMING ORGANIZATION NAME(S) AND ADDRESS(ES). Self-explanatory.

8. PERFORMING ORGANIZATION REPORT NUMBER. Enter all unique alphanumeric report numbers assigned by the performing organization, e.g. BRL-1234; AFWL-TR-85-4017-Vol-21-PT-2.

9. SPONSORING/MONITORING AGENCY NAME(S) AND ADDRESS(ES). Enter the name and address of the organization(s) financially responsible for and monitoring the work.

10. SPONSOR/MONITOR'S ACRONYM(S). Enter, if available, e.g. BRL, ARDEC, NADC.

11. SPONSOR/MONITOR'S REPORT NUMBER(S). Enter report number as assigned by the sponsoring/ monitoring agency, if available, e.g. BRL-TR-829; -215.

12. DISTRIBUTION/AVAILABILITY STATEMENT. Use agency-mandated availability statements to indicate the public availability or distribution limitations of the report. If additional limitations/ restrictions or special markings are indicated, follow agency authorization procedures, e.g. RD/FRD, PROPIN, ITAR, etc. Include copyright information.

13. SUPPLEMENTARY NOTES. Enter information not included elsewhere such as: prepared in cooperation with; translation of; report supersedes; old edition number, etc.

14. ABSTRACT. A brief (approximately 200 words) factual summary of the most significant information.

15. SUBJECT TERMS. Key words or phrases identifying major concepts in the report.

16. SECURITY CLASSIFICATION. Enter security classification in accordance with security classification regulations, e.g. U, C, S, etc. If this form contains classified information, stamp classification level on the top and bottom of this page.

17. LIMITATION OF ABSTRACT. This block must be completed to assign a distribution limitation to the abstract. Enter UU (Unclassified Unlimited) or SAR (Same as Report). An entry in this block is necessary if the abstract is to be limited.

REPORT OUTLINE – YEAR 3

Technical findings

1. Bonding effects on the slip differences in the B1 monocarbides
2. Influence of carbon vacancy formation on the elastic constants and hardening mechanisms in transition metal carbides
3. *Ab Initio* Investigations of the Phase Stability in Tantalum Carbides

Dissemination of Research Findings

Honors/Awards

Technical findings:

1. Bonding effects on the slip differences in the B1 monocarbides

Nicholas De Leon[1], Xiao-xiang Yu[1], Hang Yu[2], Christopher R. Weinberger[2], and Gregory B. Thompson[1*]

[1]The University of Alabama, Department of Metallurgical & Materials Engineering, Box 870202, Tuscaloosa, AL 35401-0202
[2]Drexel University, Department of Mechanical Engineering and Mechanics, 3141 Chestnut Street, Philadelphia, PA 19104
*Correspondence to: gthompson@eng.ua.edu
**Accepted in PRL, 2015

Abstract:
Differences in plasticity are usually attributed to significant changes in crystalline symmetry or the strength the inter-atomic bonds. In the B1 monocarbides, differences in slip planes exist at low temperatures despite having the same structure and very similar bonding characteristics. Our experimental results demonstrate concretely that HfC slips on {110} planes while TaC slips on {111} planes. Density functional theory calculations rationalize this differences through the formation of an intrinsic stacking fault on the {111} planes, formation of Shockley partials, and enhanced metallic bonding because of the valence filling of electrons between these transitional metal carbides.

Main body:

Plasticity and ductility are generally associated with crystalline symmetry and the strength of the inter-atomic bonds [1]. For example, face centered cubic (FCC) and hexagonal close packed (HCP) materials have equivalent packing with similar types of bonding but show dramatic differences in deformation because of the availability of slip systems associated with their symmetry. Alternatively, dramatic differences in bonding, such as those between ceramics and metals, can also have a similar impact on dislocation slip and ductility, but such differences are confounded by variances in symmetry. What can be even more perplexing are materials that

exhibit equivalent symmetry and bonding but show differences in deformation responses. In this letter, we explore how a subtle difference in bonding behavior regulates the slip response in two equivalently structured and similarly bonded monocarbides by combining density functional theory (DFT) and experimental results. Our findings debunk how prior hard sphere based models are not able to rationalize experimental findings. Through the use of these modern computational tools, we elucidate how bonding, along with symmetry, regulates slip in this class of transition metal monocarbides (TMMCs).

The group IVB and VB monocarbides provide a perfect test-bed to explore subtle differences in bonding and its role in mechanical properties. Both groups of TMMCs form the B1, or rocksalt structure, which is an array of FCC metal atoms with the carbon atoms filling every octahedral interstice [2,3]. The bonding in these materials is a mix of covalent, metallic and ionic resulting in high hardness as well as good thermal and electrical conductivity [4-7]. The materials are generally brittle at room temperature and exhibit remarkable ductility at elevated temperatures [8-10].

The last comprehensive summary of plastic deformation of TMMCs was written by Rowcliffe in 1984 [11], where most slip systems were determined using hardness anisotropy. This work reported that the dominant slip systems in the group IVB monocarbides are a/2<110>{110} while the group VB monocarbides revealed a/2<110>{111} at room temperature. Rowcliffe et al. [12] also noted that the group IVB TMMCs were significantly more brittle than the group VB TMMCs, which is attributed to the number of available independent slip systems in the dominant family, i.e. two for the a/2<110>{110} and five for a/2<110>{111}. The supplemental material of this letter provides a review and summary table which shows both slip systems are found in all of the materials [13]. However, it has been established from past experiments [8,11,14-16] that one family of slip system appears to be dominant for each type of carbide, i.e. the {110} in the group IVB TMMCs and {111} in the group VB TMMCs. Though these differences have been known for decades, the change in slip systems across the TMMCs has perplexed scientists for equally as long.

To eliminate differences in homologous temperatures, we pick the two monocarbides with nearly equivalent melting temperatures, HfC (~3900 ^{o}C) and TaC (~3880 ^{o}C), to conduct our studies. The deformation of TaC has been well investigated across a number of temperatures establishing its preference to slip on {111} planes through indentation experiments and elevated temperature creep studies [11,16]. Despite the well-known preference for slip on {111} planes, the mechanism controlling slip is not well known. Authors have suggested a simple high lattice friction model with dislocations splitting into Shockley partials, a synchro-shear mechanism regulated by carbon diffusion, as well as motion via zonal dislocations to rationalize experimental observations [9,11,17]; the latter two being unlikely to occur during room temperature deformation. In addition, as the carbon concentration in TaC_{1-x} is reduced, hardness anisotropy measurements indicated that {110} slip becomes more prevalent [18]. In contrast, there has been limited studies in HfC and few theories that explain the {110} slip in this system or other similar group IVB carbides. The typical explanation has been that these materials have more covalent bonding preventing {111} slip [11,19]. As the temperature increases, one can expect that multiple slip systems would become more favorable and a dominate slip system, as noted in lower homologous temperatures, may not be as apparent.

To verify these results obtained decades ago, we performed microindentation tests, Fig. 1(a), in nearly stoichiometric HfC and TaC at room temperature with the corresponding dislocations observed in the TEM micrographs of Figs. 1(b) and 1(c). The TEM results confirm large amounts of dislocation plasticity within the TaC grains under the indents whereas the plasticity in HfC was much more limited and confined to large grains directly under the indents with estimated dislocation densities being ~1.10 x 10^{14} m^{-2} (TaC) and ~8.83 x 10^{13} m^{-2} (HfC) under the indents and ~1.32 x10^{14} (TaC) and ~3.12 x10^{11} m^{-2} (HfC) away from the indents; the experimental details can be found in the supplementary information (SI) [13].

Dynamical diffraction TEM analysis confirmed the slip system as a/2<110>{111} in TaC and a/2<110>{110} in HfC [13]. LECO analysis confirmed nearly stoichiometric and equal amounts of carbon in the samples, eliminating this as a cause for the change in slip planes. These results, in addition to the previous observations in single crystals [12], suggest the choice of slip planes and the limited ductility in HfC compared to TaC are intrinsic properties.

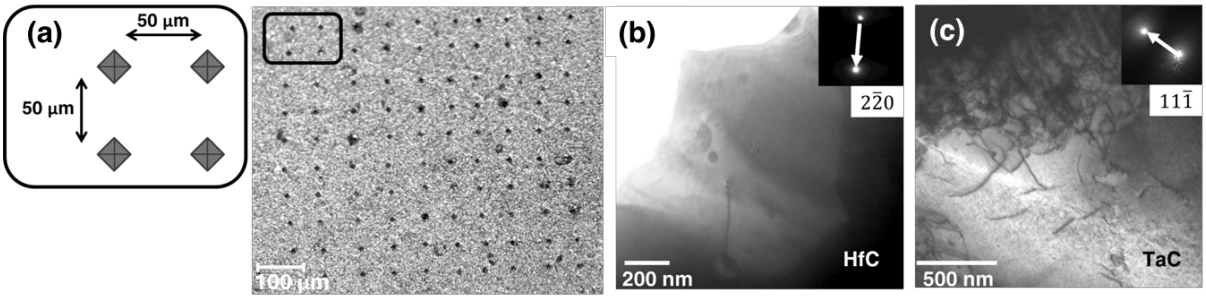

FIG. 1. (a) Representative schematic and optical micrograph of the 10x10 array of Vickers indents in a carbide specimen. TEM bright field micrographs of typical dislocation structures found in HfC (b) and TaC (c).

It is generally thought that slip will occur in the closes packed directions on the most widely spaced planes This suggests slip on {111} planes in FCC metals and {110} slip in BCC metals and is thought to control the competition between basal and prims slip in HCP metals. The other factor complicating slip is the existence of fault planes [20]. However, this can be complicated in materials with mixed bonding. The predominately held belief with regard to the differences in slip for group IVB and VB carbides was based on the hard sphere model. First proposed to be viable in ionic and covalent materials by Van Der Walt and Sole [21], Rowcliffe and Hollox [18] supported its applicability to carbides. The hard sphere model relates preferred slip to the interatomic spacing within the structure as determined by the ratio of the radii of the carbon and metal atoms. It states that perfect slip on the {110} plane is preferred in covalently bonded materials with a radius ratio (r/R) < 0.414, on the {111} plane when $0.414 \leq r/R \leq 0.633$, and on the {100} when r/R > 0.633. It also only predicts partial slip on the {111} plane at r/R > 0.732. The radius ratios of all the group IVB and VB carbides, as reported by Toth [4], along with the hard sphere model slip predictions and the experimentally reported and observed active slip systems are tabulated in the SI for the reader. These results suggest that all of the TMMCs should deform via {111} slip despite the observations of the {110} slip dominance in

the group IVB TMMCs. Given the close radius ratio between TiC and the group VB TMMCs, the model has difficulty even predicting trends. It is evident that the hard sphere model does not adequately explain or predict favorable slip within the TMMCs even though it has been propagated for several years in contrast to prior experimental data. Moreover it further breaks down when partial slip is added to the discussion as will be elucidated shortly.

To provide for a more accurate understanding of slip, we have employed first principle DFT calculations of the generalized stacking fault (GSF) energies (see SI). The GSF energy surfaces for perfect slip for {110} and {111} planes are plotted in Fig. 2(a). It was found that in either TMMC system, {110} slip was more energetically favorable than {111} when compared along the <110> direction. Moreover TaC was shown to have a lower GSF than HfC, which helps explain the higher dislocation densities noted in the material between the two carbides, Fig. 1. Though TaC has a lower GSF energy than HfC, this does not explain its dominance on {111} planes, as perfect slip on these planes are nearly two-fold higher in energy than {110} perfect slip, Fig. 2(a). The choice of slip planes rather lies with the presence of an intrinsic fault, Fig. 2(b), and ability of the perfect dislocations to split into Shockley partials, Figs. 2(c) and 2(d).

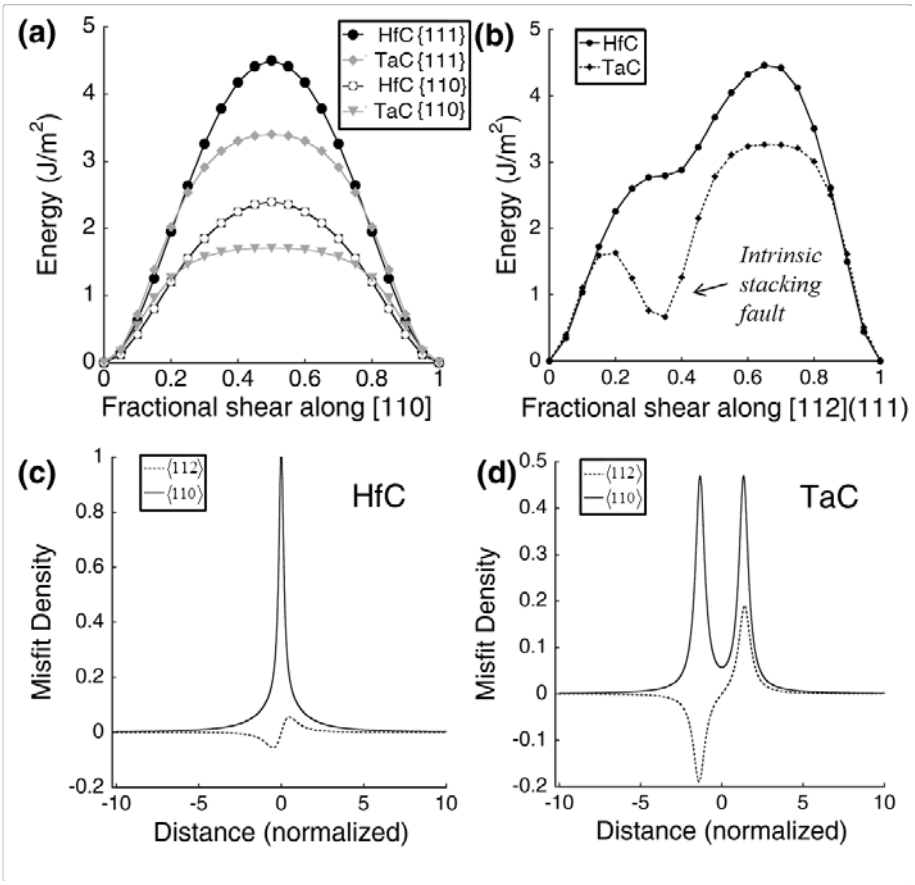

FIG. 2. DFT calculated generalized stacking fault energy curves for fractional shear along (a) [110] on both (111) and (110) planes and (b) for the partial dissociation [112](111) for both HfC and TaC. Note the intrinsic stacking fault in TaC which is absent in HfC. Associated PN model misfit density plots for (c) HfC and (d) TaC, with the distance normalized by the Burgers vector. The preference for splitting into partials is evident in TaC and not HfC.

It is well known that dislocations in close-packed metals, amongst others, dissociate into partial dislocations to reduce the elastic energy of the system [20]. To explore this possibility in the TMMCs, we computed the <112>{111} GSF curves for HfC and TaC, Fig. 2(b). In this configuration a local 1D minima in TaC, known as an intrinsic stacking fault (ISF), is noted but is absent in HfC. This ISF was noted to be present in all of the group VB TMMCs but absent in the group IVB TMMCs (see SI) [13], indicting uniformity across the two family classes of monocarbides [13]. The ISF, when present, represents a metastable minimum energy configuration in the energy surface, which may result in the splitting of perfect dislocations into partial dislocations. The unstable stacking fault energy (USF) is the maximum energy along the minimum energy path and can indicate the relative ductility of a material [22,23]. In the hard sphere model, an ISF is only present for radius ratios or $r/R > 0.732$, when the hard sphere model predicts {001} slip. The presence of an ISF in TaC, which would correspond to {001} slip in the hard sphere model, is a direct indication of a fundamental breakdown of the hard sphere model. Moreover, the presence of a stable ISF also likely contributes to the phase stability of faulted-phases, such as Ta_4C_3, in sub-stoichiometric tantalum carbides but such phases are not observed in the hafnium carbides [24].

These DFT calculations shed new light into the differences in the room temperature slip behavior between the two carbides that has been lacking for years. Perfect slip on the {110} surface is energetically most favorable for HfC, which is in agreement with the results reported here and elsewhere [11]. In contrast, TaC can supersede the {110} slip because of its favorable ISF on the {111} plane, which is absent in HfC.

To confirm that dislocations dissociate into partials in TaC on the {111} plane, we used a Peierls-Nabarro (PN) model to compute the potential for dislocation dissociation. These results are shown in Figs. 2(c) and 2(d) and confirm our expectations based on the GSF curves alone. A TaC dislocation will split slightly into partial dislocations on the {111} plane as shown by the separate peaks in Fig. 2(d). In contrast, the lack of the ISF prevents dislocations from splitting in HfC, also confirmed by our PN model in Fig. 2(d). Hence, the dissociation of the dislocations helps stabilize them on the {111} plane and generally lowers their barrier to motion making {111} slip more prevalent in TaC than HfC.

To fully understand how the DFT calculations can provide an alternate explanation to the hard sphere model concepts, one must consider the nature and directionality of the bonding within the carbides. Fig. 3 shows the isoconcentration charge surfaces computed from our DFT simulations, providing a visual aid in highlighting the differences in the bonding between the carbides during the shear process. In all renderings, the isocharge surfaces were equivalent for direct visual comparison purposes [13]; see SI for details

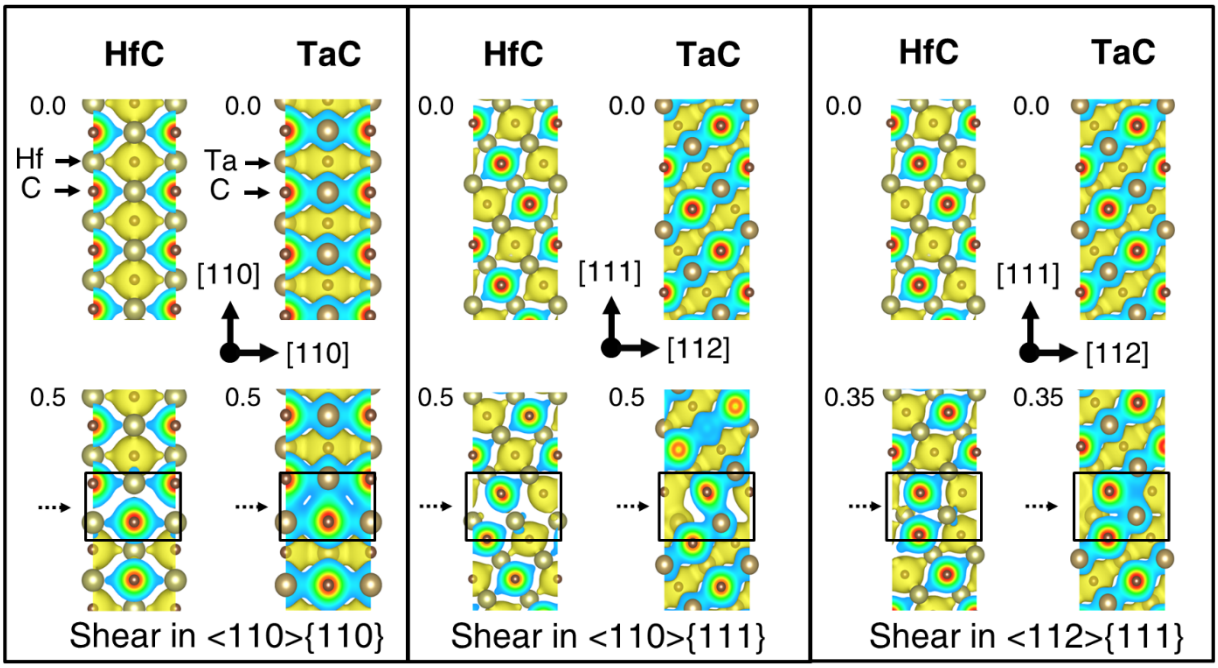

FIG. 3. DFT isoconcentration charge surfaces for HfC and TaC in a zero and fraction shear state for various slip conditions. The dash arrow indicates the fault plane highlighted by the solid box region. The top row are the unsheared conditions with the bottom row are the designated shear indicated by the fraction value. The compass arrows indicate the viewing prospective.

In the un-sheared state, we can clearly see a difference the bonding that occurs in these two carbides. Notably, the isocharge surfaces are more diffuse between the atoms in TaC than in HfC regardless of the isocharge value used in the visualization. This indicates a less directional bond and thus more metallic-like character. This is a direct consequence of the extra valence electron contributed by tantalum, a group VB transition metal atom, to the Ta-C bond. The difference in bonding is further highlighted as the crystal shears, with the bonding behaving in a more localized fashion in HfC than TaC, i.e. compare the charge distribution between the two shear planes (dashed arrows) for the 0.5 shear along the <110>{110}.

The less directional nature of the bonds in TaC also allows for the stabilization of the ISF. The isocharge surfaces at a fractional shear of 0.35 in the a/6<112> direction on the {111} planes, Fig. 3, exhibit a rotation of the bonds for both TaC and HfC. As the top half of the crystal shears relative to the bottom half via a Shockley partial dislocation, the bonds between the metal atoms and carbon atoms in this plane undergo a 60 degree rotation about the plane normal. This bonding rotation increases the bond energy which will be a function of the angular nature of the bonds themselves. The less directional nature of the Ta-C bonds helps to mitigate the energy penalty for this bond rotation. Clearly, the extra *d*-shell valance electron of tantalum dramatically helps to stabilize the fault as compared to hafnium. Since both systems have equivalent coordination environments (bond hybridization), the extra *d* valance electron provides for some charge delocalization upon rotation and would explain the universality for a stabilized ISF in all of the other group VB TMMCs shown in the SI [13].

This faulted configuration stacks the metal atoms over the metal atoms and the carbon atoms over the carbon atoms across the fault. In other words, the atoms directly in the fault have a trigonal prismatic coordination with respect to the other species and tetrahedral coordination with respect to their own atom type. It has been previously suggested that in the synchro-shear mechanism [17,25,26], the tetrahedral coordination of the metal atoms would be unfavorable. This would be correct for HfC but not necessarily true for TaC, where an ISF is favorable because of the nature of its bonds. Finally, it is interesting to note that their appears to be some bonding between carbon atoms in the TaC ISF though this is likely an artifact to the sensitivity of the exact isocharge value used in visualization. Similar stabilization of ISF energies has been noted with metallic alloys where the solute atoms contribute excess valence electrons to the system [27].

In summary, a series of room temperature indents in HfC and TaC were characterized using TEM dynamical diffraction analysis to determine the operating slip planes in these materials. We confirmed that $a/2\langle 110\rangle$ {110} slip occurs in HfC and $a/2\langle 110\rangle$ {111} slip in TaC at room temperature, with two orders of magnitude higher density of dislocations observed in TaC than HfC. Using DFT, the GSF curves for {110} and {111} slip were computed revealing that perfect {110} slip was more favorable with TaC having a lower energy for slip than HfC. This result confirmed the dominant slip system observed in HfC and the higher dislocation density seen in TaC for equivalent room temperature indents. The presence of an ISF in TaC promotes the dissociation of perfect dislocations into partials on the {111} plane, which allowed it to bypass {110} slip. The extra electron in TaC as compared to HfC provides a more metallic nature to the bonds [6,7] enhancing slip and stabilizing the ISF. Coupling prior experimental work in the other group IVB and VB TMMCs where different dominate slips planes have been reported [11,14-16] with their similar GSF curves (see SI), we have concluded that the slip variation is likely contributed to the ability to or not to form an ISF. The stability of this ISF appears to be related to the excess d-shell electron between these two groups of TMMCs. The operation of {111} slip allows for a larger number independent slip systems (i.e. 5) compared to {110} slip (i.e. 2), further enhancing ductility of the material and changing its macroscopic properties. This suggest that engineering the stacking fault energy to access or limit specific deformation modes through solute alloying could allow for the future design of tunable hardness in these carbides beyond using simple elastic constant criteria [28-30].

Acknowledgments:

This research was supported under the Air Force Office of Scientific Research under grant FA9550-12-1-0104 DEF, Dr. Ali Sayir Program Manager; the Central Analytical Facility supported by The University of Alabama Office for Research; and lastly, the high performance computing resources and technical support from the Alabama Supercomputer Authority is recognized.

References and Notes:

[1] G. E. Dieter and D. Bacon, *Mechanical metallurgy* (McGraw-Hill New York, 1986), 3 edn.
[2] E. K. Storms, in *The Refractory Carbides* (Academic Press, 1967).
[3] G. Santoro and H. B. Probst, in *Advances in X-ray Analysis: Proceedings of the 12th Annual Conference on Applications of X-ray Analysis*, edited by W. M. Mueller, G. Mallett, and M. Fay (Plenum Press, 1963).
[4] L. E. Toth, *Transition Metal Carbides and Nitrides* (Academic Press, New York, 1971).
[5] W. S. Williams, Prog. Solid State Chem. **6**, 57 (1971).
[6] F. Viñes, C. Sousa, P. Liu, J. A. Rodriguez, and F. Illas, J. Chem. Phys. **122**, 174709 (2005).
[7] Y. Liu, Y. Jiang, R. Zhou, and J. Feng, J. Alloys Compd. **582**, 500 (2014).
[8] A. Kelly and D. J. Rowcliffe, J. Am. Ceram. Soc. **50**, 253 (1967).
[9] G. E. Hollox, Mater. Sci. Eng. **3**, 121 (1968).
[10] R. Steinitz, in *Conference on Nuclear Applications of Nonfissionable Ceramics*, edited by A. Boltax, and J. H. Handwerk (American Nuclear Society, Washington, D.C., 1966), p. 75.
[11] D. J. Rowcliffe, in *Deformation of Ceramic Materials II*, edited by R. Tressler, and R. Bradt (Springer US, 1984), pp. 49.
[12] D. J. Rowcliffe and G. E. Hollox, J. Mater. Sci. **6**, 1261 (1971).
[13] See Supplemental Material at [URL will be inserted by publisher] for detailed methodology and additional results which includes Refs. [31-42].
[14] D. W. Lee and J. S. Haggerty, J. Am. Ceram. Soc. **52**, 641 (1969).
[15] G. Morgan and M. H. Lewis, J. Mater. Sci. **9**, 349 (1974).
[16] C. Kim, G. Gottstein, and D. S. Grummon, Acta Metall. Mater. **42**, 2291 (1994).
[17] M. H. Lewis, J. Billingham, and P. S. Bell, in *Electron Microscopy and Structure of Materials, Proceedings of the 5th International Materials Symposium*, edited by G. Thomas, R. Fulrath, and R. M. Fisher (University of California Press, 1971), pp. 1084.
[18] D. J. Rowcliffe and G. E. Hollox, J. Mater. Sci. **6**, 1270 (1971).
[19] R. H. J. Hannink, D. L. Kohlstedt, and M. J. Murray, Proceedings of the Royal Society of London. Series A, Mathematical and Physical Sciences **326**, 409 (1972).
[20] J. P. Hirth and J. Lothe, *Theory of Dislocations* (Krieger, Malabar, 1982).
[21] C. M. Van Der Walt and M. J. Sole, Acta Metall. **15**, 459 (1967).
[22] J. R. Rice and G. E. Beltz, Journal of the Mechanics and Physics of Solids **42**, 333 (1994).
[23] S. Ogata, J. Li, N. Hirosaki, Y. Shibutani, and S. Yip, Phys. Rev. B **70**, 104104 (2004).
[24] X. X. Yu, C. R. Weinberger, and G. B. Thompson, Acta Mater. **80**, 341 (2014).
[25] J. Hornstra, Journal of Physics and Chemistry of Solids **15**, 311 (1960).
[26] M. L. Kronberg, Acta Metall. **5**, 507 (1957).
[27] X.X. Yu and C.Y. Wang, Acta Mater. **57**, 5914 (2009).
[28] H. Li, L. Zhang, Q. Zeng, H. Ren, K. Guan, Q. Liu, and L. Cheng, Solid State Commun. **151**, 61 (2011).
[29] D. Varshney, S. Shriya, and N. Singh, AIP Conference Proceedings **1512**, 1016 (2013).
[30] X.X. Yu, G. B. Thompson, and C. R. Weinberger, Journal of the European Ceramic Society **35**, 95 (2015).
[31] edited by N. A. Laboratories13 Delta Drive #4 Londonderry, NH 03053.

[32] E. Rudy and D. P. Harmon, *AFML-TR-65-2, Part I, Volume V* (Air Force Materials Laboratory Research and Technology Division, Air Force Command, Wright-Patterson A.F.B., Ohio, 1965).
[33] G. Ravichandran and G. Subhash, Int. J. Solids Struct. **32**, 2627 (1995).
[34] J. W. Edington, *Practical electron microscopy in materials science* (N.V. Philips' Gloeilampenfabrieken, Eindhoven, 1976).
[35] R. K. Ham, Philosophical Magazine **6**, 1183 (1961).
[36] F. R. Castro-Fernáandez and C. M. Sellars, Philosophical Magazine A **60**, 487 (1989).
[37] P. E. Blöchl, Phys. Rev. B **50**, 17953 (1994).
[38] G. Kresse and J. Furthmüller, Phys. Rev. B **54**, 11169 (1996).
[39] J. P. Perdew, K. Burke, and M. Ernzerhof, Phys. Rev. Lett. **77**, 3865 (1996).
[40] A. L. Bowman, J. Phys. Chem. **65**, 1596 (1961).
[41] W. B. Pearson, P. Villars, L. D. Calvert, and W. B. Pearson, *Pearson's handbook of crystallographic data for intermetallic phases / by P. Villars and L.D. Calvert* (Metals Park, Oh : American Society for Metals, c1985., 1985), Vol. 2.
[42] V. V. Bulatov and W. Cai, *Computer simulations of dislocations / Vasily V. Bulatov, Wei Cai* (Oxford ; New York : Oxford University Press, 2006., 2006), Oxford series on materials modelling: 3.

Supplementary Material for: Bonding effect on the slip differences in the B1 monocarbides

I. EXPERIMENTAL DETAILS

A. Sample Fabrication

The HfC and TaC test bars were produced by Exothermics Inc. using stoichiometric monocarbide powders which was mechanically pressed and evacuated in a tantalum container termed a 'can'. The can was subjected to Hot Isostatic Pressing (HIP) at 200 MPa and 1600 ^{o}C for 100 minutes in an argon atmosphere. Stoichiometry was maintained during the HIP process, which was confirmed ($HfC_{0.992}$ and $TaC_{0.994}$) by LECO combustion and infrared analysis [1] of the samples' carbon content. The post-HIP billets had a density of ~98% measured by a water emersion displacement technique and compared to the theoretical densities of 12.76 g/cc for HfC and 14.8 g/cc for TaC [2].

B. Indentation and Microscopy Preparation

TEM foils were prepared by ultrasonically drilling 3 mm discs from slices of the HIP'ed billets using a Fischione Instruments Model 170 drill with a SiC abrasive slurry. The discs were then mechanically ground to < 100 μm using SiC and then indented to induce room temperature deformation. A 10 x 10 matrix of 100 Vicker's microhardness indentations using a 300 g load for 5 seconds were made in the center of each specimen which translates to a strain rate of approximately 10^{-3} s^{-1}. This process of indentation is similar to the method employed by Kim et. al [3]. In general, ceramics have been shown to be strain rate insensitive for rates < 10^{+3} s^{-1} [4]. For this test, we were in the standard quasi-static strain rate and our results should be universal over similar ranges of conditions.

The un-indented sides were then dimpled to < 15 μm with 6 μm diamond paste polish under a rotating 15 mm diameter steel wheel using a Fischione Instruments Model 200 unit. The dimpled discs were Argon ion milled to electron transparency using a Gatan Precision Ion Polishing System (PIPS®). The PIPS® dual guns were operated at 3 keV per gun and aligned at contrary incident milling angles of 8° to achieve perforation. The guns were operated at 2 keV and 6° for a final 'clean-up' step. The specimens were continuously rotated during the ion milling.

C. Electron Microscopy

Conventional dynamical TEM was performed with a FEI F20 Tecnai (S)TEM operated at 200 keV. The Burgers vectors were determined by conventional $\mathbf{g} \cdot \mathbf{b} \times \mathbf{u}$ analysis, where **g** is the diffraction vector, **b** is the Burgers vector of the dislocation and **u** is the line sense of the dislocation [5]. In Fig. S1(a), the two groups of parallel dislocations in the indented HfC specimen are clearly visible using the $(\bar{2}00)$ reflection condition taken off the $[001]$ zone axis. Upon tilting to the $(0\bar{2}0)$, Fig. S1(c), and $(\bar{1}31)$, Fig. S1(f), reflections, these groups of dislocation become invisible while a perpendicular group revealed itself. The inset images in Fig. S1 are the two-beam conditions for each respective image. The consistent Burgers vector identified under these conditions for the dislocation is the common $\mathbf{b} = a/2\langle 110 \rangle$ type. Considering this Burgers vector and other visibility conditions taken from two-beam conditions off the $[\bar{1}\bar{1}2]$ and $[0\bar{1}1]$ zone axes, the consistent and stereographically confirmed slip plane was identified to be $\{110\}$ type. In Fig. S1(h) many dislocations in the indented TaC specimen are clearly visible using the $(11\bar{1})$ reflection condition taken from the $[112]$ zone axis. The dislocations of interest are the long segments that ran parallel to the edge of the sample. Upon tilting to the $(\bar{1}1\bar{1})$ reflection, Fig. S1(l), the dislocations become invisible. The consistent Burgers vector identified under these conditions for the dislocations is the common $\mathbf{b} = a/2\langle 110 \rangle$ type. Considering this Burgers vector, other visibility conditions taken from two-beam conditions from the $[111]$ and $[011]$ zone axes. The consistent and stereographically confirmed slip plane was identified to be $\{111\}$ type.

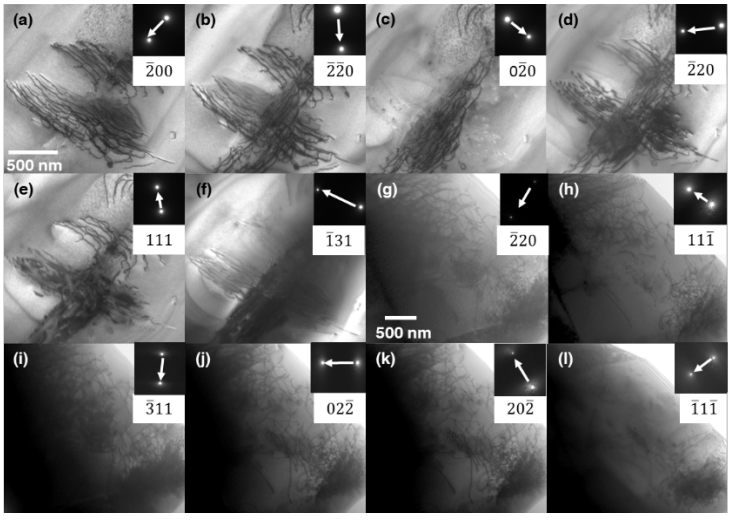

FIG. S1. BF-TEM images with associated two-beam conditions in the inset. Room temperature indented HfC images are (a)-(f), which correspond to the visibility conditions found in Table S1. Room temperature indented TaC are (g)-(l), which correspond to the visibility conditions found in Table S2.

TABLE S1. “Visibility Table” for HfC tilt experiment.

	Possible Burgers vectors (±, times a/2)						
g (hkl)	$[110]$	$[1\bar{1}0]$	$[101]$	$[10\bar{1}]$	$[011]$	$[01\bar{1}]$	Visibility
$\bar{2}00$	1	1	1	1	0	0	V
$\bar{2}\bar{2}0$	2	0	1	1	1	1	V
$0\bar{2}0$	1	1	0	0	1	1	I
$\bar{2}20$	0	2	1	1	1	1	V
111	1	0	1	0	1	0	V
$\bar{1}31$	1	2	0	1	2	1	I

TABLE S2. “Visibility Table” for TaC tilt experiment.

	Possible Burgers vectors (±, times a/2)						
g (hkl)	$[110]$	$[1\bar{1}0]$	$[101]$	$[10\bar{1}]$	$[011]$	$[01\bar{1}]$	Visibility
$\bar{2}20$	0	2	1	1	1	1	V
$11\bar{1}$	1	0	0	1	0	1	V
$\bar{3}11$	1	2	1	2	1	0	V
$02\bar{2}$	1	1	1	1	0	2	V
$20\bar{2}$	1	1	0	2	1	1	V
$\bar{1}1\bar{1}$	0	1	1	0	0	1	I

The dislocation densities, ρ, were estimated to compare of regions near an indent versus regions farther from an indent. This was performed using the line intercept calculation as outlined by Ham [6] and by Castro-Fernaandez et al. [7] where n is the number of intersections, L is the length of the grid, and t is the thickness, seen in equation 1.

$$\rho = \frac{2n}{Lt} \tag{1}$$

It would be reasonable to expect the dislocation density to decrease in areas away from an indent for a brittle material at room temperature. In areas near indentations, $\rho_{HfC} = 8.83 \times 10^{13}$ m^{-2} and $\rho_{TaC} = 1.10 \times 10^{14}$ m^{-2}, values one would expect for a worked material. On the other hand, in areas farther away from the indents, $\rho_{HfC} = 3.12 \times 10^{11}$ m^{-2} and $\rho_{TaC} = 1.32 \times 10^{14}$ m^{-2}, showing a marked drop in dislocation activity for only HfC, consistent with the report of HfC being more brittle than TaC under indentation by Rowcliffe et al. [8].

II. HARD SPHERE MODEL

The hard sphere model suggested by Van Der Walt and Sole is based on the principle of minimum uplift. The amount of uplift, normal to a given crystallographic plane, required to move the atoms in the Burgers vector direction depends on the radius ratio of the two species in the rocksalt structure. The authors showed that this would predict {110} slip for radius ratios of r/R

< 0.414, {111} slip for 0.414<r/R<0.633 and {001} slip for r/R > 0.633. Note that the model also predicts an ISF on the {111} plane when r/R > 0.732, which should never be relevant since the model would suggest {001} slip. This model was correlated to the slip planes in ionic rocksalt materials at later extended to the cubic monocarbides by Rowcliffe and Hollox [9], however these materials are dominated by covalent and metallic bonding, which may preclude its use. Using the ionic radius ratios of Toth [10], the predictions of the hard sphere model are shown in Table S3 along with the reported slip planes.

TABLE S3. Hard sphere model slip predictions compared to observed systems, group IVB and VB carbides. Its predictions are shown to be incomplete. (*Rowcliffe [11], [+]Lee [12], [#]Morgan [13], [&]Kim [3], [%]This work)

	Compound	Radius Ratio r/R	Hard Sphere Model Slip prediction	Observed Slip
IVB	TiC	0.526	111	110*, 111*
	ZrC	0.483	111	110*[+], 111[+], 100[+]
	HfC	0.486	111	110*[%], 111[%]
VB	VC	0.576	111	110*, 111*
	NbC	0.530	111	110*, 111*[#]
	TaC	0.529	111	110[%], 111*[&]

III. COMPUTATIONAL METHODS

A. Generalized Stacking Fault Energies

The simulations of HfC and TaC were conducted using DFT as implemented in the Vienna ab initio Simulation Package (VASP). A projector augmented wave (PAW) potential [14] was used to describe the interaction between the valence electrons and the ionic cores. The Perdew-Burke-Ernzerhoff (PBE) [15,16] exchange correlation functions within the generalized gradient approximation (GGA) were used for evaluation of the exchange-correlation energy. Parametric testing indicated that an energy cut-off of 400 eV was sufficient for all calculations and the energy convergence threshold was set to 1e-4 eV. The calculated lattice parameters that were arrived at using a Murnaghan fit for the relaxed HfC (4.65 Å) and TaC (4.47 Å) crystals were in good agreement with the experimental values determined via x-ray diffraction (4.64 Å and 4.47 Å, respectively) [17,18] when a sufficiently large Monkhorst-Pack k-point scheme was used (11x11x11) along with ion relaxation for a single unit cell.

Using the lattice parameters determined, supercells with 24 to 30 atomic layers were constructed where the crystallographic plane of interest was aligned parallel to the x-y simulation

axes, (111) and (110), respectively. A disregistry plane was created in the middle of the supercell, where all the atoms above were rigidly shifted. The GSF energy was obtained by calculating the increased amount of energy in the system relative to the base, un-shifted structure, while relaxing all but the top and bottom two layers of atoms in the supercell with respect z axis. The top and bottom two layers remained fixed in all directions. The k-point meshes were chosen to be inversely proportional to the real space length in that direction such the ratio of 11 k-points to the lattice parameter was approximately maintained. Since the simulations use periodic boundary conditions, a 15 Å gap was placed parallel to the disregistry plane so that only one stacking fault would be present.

The DFT GSF curves for HfC and TaC are shown in the manuscript in Fig. 2. The unstable stacking fault energy (USF) for the <110>{110} slip is 2.4 and 1.7 J/m^2 for HfC and TaC respectively. This increases to 4.5 and 3.4 J/m^2 for <110>{111} slip in HfC and TaC. In TaC, the intrinsic stacking fault energy is found to be 0.6 J/m^2 and the USF between the equilibrium and ISF was 1.6 J/m^2, the lowest of any surface. There is no ISF in the case of HfC and the USF is 2.8 J/m^2. The remaining GSF curves for the group IVB and VB monocarbides are shown in Fig. S2. The equivalent trends of an ISF present in the group VB monocarbides that is not present in the group IVB monocarbides is observed indicating the universal nature associated with the differences in slip between these two equivalent symmetry carbides.

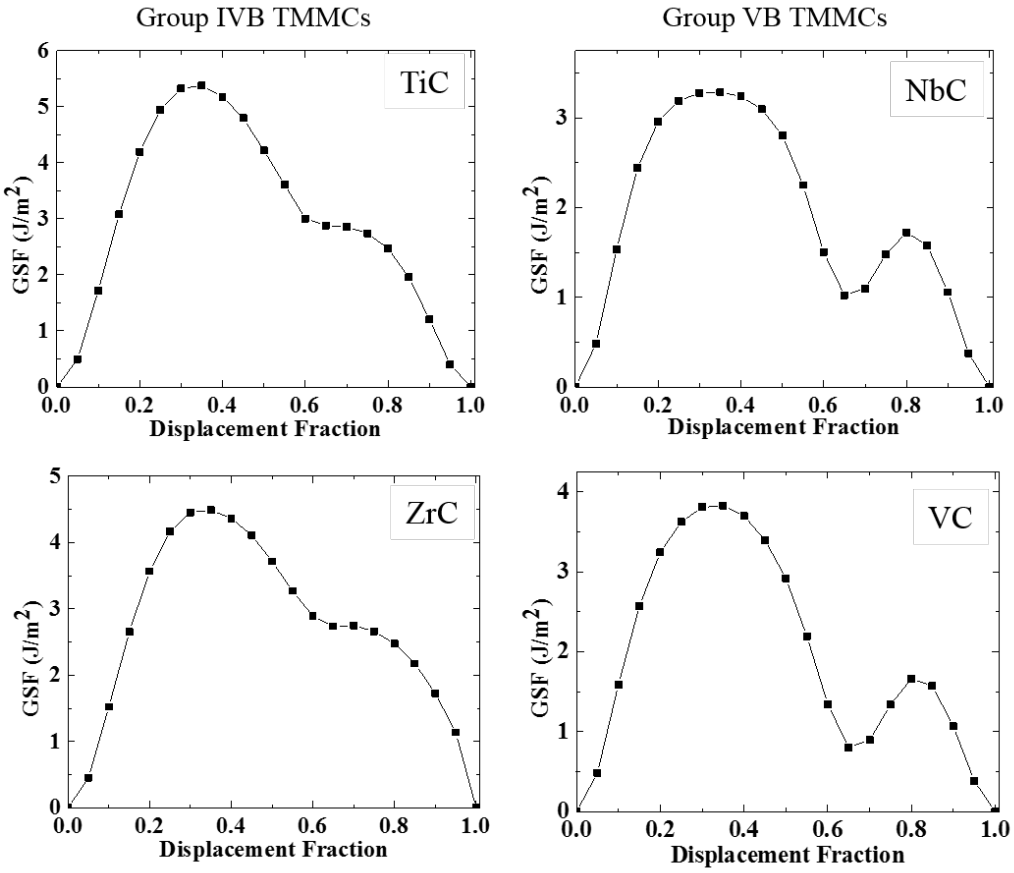

FIG. S2. GSF curves for the various group IVB and VB transition metal monocarbides (TMMCs). Note the ISF present in the group VB series that is absent in the group IVB series.

B. Peierls-Nabarro Model

To model the dissociation of the dislocation on the {111} plane, a standard Peierls Nabarro model [19] was implemented. The model treats planar dislocation core deformation by accounting for the elastic energy, E_{el}, and misfit energy, E_{msft}, where the core structure was determined by minimizing the total energy, E_{tot}. This relationship is shown in equations (2) and (3),

$$E_{tot}[u(x)] = E_{el} + E_{msft} \quad (2)$$

$$E_{tot}[u(x)] = -K \int_{-R}^{R} \int_{-R}^{R} \rho(x)\rho(x') \ln|x - x'| \, dxdx' + \int_{-R}^{R} \gamma\big(u(x)\big)dx \quad (3)$$

where $u(x)$ is the misfit across the cut plane, R is the cut-off radius, $\rho(x)$ is the disregistry density, $\gamma(u(x))$ is the misfit potential, and K is a constant represent the material properties and the dislocation type. For a screw dislocation, $K_s = \mu/4\pi$ and $K_e = \mu/(4\pi(1-\nu))$ for an edge dislocation, where μ is the shear modulus and ν is the Poisson's ratio for the material.

By choosing the trial functions of equations (4) and (5),

$$u_x(x) = \frac{b}{\pi}\left(A_1 \arctan\frac{x-x_1}{c_1} + A_2 \arctan\frac{x-x_2}{c_2}\right) \quad (4)$$

$$u_z(x) = \frac{b}{\pi}\left(A_3 \arctan\frac{x-x_3}{c_3} + A_4 \arctan\frac{x-x_4}{c_4}\right) - \frac{b}{2} \quad (5)$$

where b is the Burgers vector, x_i is the distance from the dislocation core, c_i is the optimization parameter, and A_i is a proportional constant, and following the relationship of equation (6), we can also derive the trial functions for the disregistry densities, shown in equations (7) and (8).

$$\rho(x) = \frac{du_x(x)}{dx} \quad (6)$$

$$\rho_x(x) = \frac{b}{\pi}\left(\frac{A_1 c_1}{(x-x_1)^2 + c_1^2} + \frac{A_2 c_2}{(x-x_2)^2 + c_2^2}\right) \quad (7)$$

$$\rho_z(x) = \frac{b}{\pi}\left(\frac{A_3 c_3}{(x-x_3)^2 + c_3^2} + \frac{A_4 c_4}{(x-x_4)^2 + c_4^2}\right) \quad (8)$$

Notice that the <*x, z*> notation represents the direction. Plane <*x, z*> represents a {111} plane in the crystal and *x*-direction corresponds to a <110> direction and the *z*-direction corresponds to a <112> direction.

C. Isocharge Rendering

The isocharge values for the renderings shown in Fig. 3. of the manuscript were done using a value of 0.04 e/Bohr^3. The maximum contour corresponds to 0.12 e/Bohr^3 while the minimum is that used to draw the isosurface.

References

[1] edited by N. A. Laboratories13 Delta Drive #4 Londonderry, NH 03053.

[2] E. Rudy and D. P. Harmon, *AFML-TR-65-2, Part I, Volume V* (Air Force Materials Laboratory Research and Technology Division, Air Force Command, Wright-Patterson A.F.B., Ohio, 1965).

[3] C. Kim, G. Gottstein, and D. S. Grummon, Acta Metall. Mater. **42**, 2291 (1994).

[4] G. Ravichandran and G. Subhash, Int. J. Solids Struct. **32**, 2627 (1995).

[5] J. W. Edington, *Practical electron microscopy in materials science* (N.V. Philips' Gloeilampenfabrieken, Eindhoven, 1976).

[6] R. K. Ham, Philosophical Magazine **6**, 1183 (1961).

[7] F. R. Castro-Fernáandez and C. M. Sellars, Philosophical Magazine A **60**, 487 (1989).

[8] D. J. Rowcliffe and G. E. Hollox, J. Mater. Sci. **6**, 1261 (1971).
[9] D. J. Rowcliffe and G. E. Hollox, J. Mater. Sci. **6**, 1270 (1971).
[10] L. E. Toth, *Transition Metal Carbides and Nitrides* (Academic Press, New York, 1971).
[11] D. J. Rowcliffe, in *Deformation of Ceramic Materials II*, edited by R. Tressler, and R. Bradt (Springer US, 1984), pp. 49.
[12] D. W. Lee and J. S. Haggerty, J. Am. Ceram. Soc. **52**, 641 (1969).
[13] G. Morgan and M. H. Lewis, J. Mater. Sci. **9**, 349 (1974).
[14] P. E. Blöchl, Phys. Rev. B **50**, 17953 (1994).
[15] G. Kresse and J. Furthmüller, Phys. Rev. B **54**, 11169 (1996).
[16] J. P. Perdew, K. Burke, and M. Ernzerhof, Phys. Rev. Lett. **77**, 3865 (1996).
[17] A. L. Bowman, J. Phys. Chem. **65**, 1596 (1961).
[18] W. B. Pearson, P. Villars, L. D. Calvert, and W. B. Pearson, *Pearson's handbook of crystallographic data for intermetallic phases / by P. Villars and L.D. Calvert* (Metals Park, Oh : American Society for Metals, c1985., 1985), Vol. 2.
[19] V. V. Bulatov and W. Cai, *Computer simulations of dislocations / Vasily V. Bulatov, Wei Cai* (Oxford ; New York : Oxford University Press, 2006., 2006), Oxford series on materials modelling: 3.

2. Influence of carbon vacancy formation on the elastic constants and hardening mechanisms in transition metal carbides

Xiao-Xiang Yu[a], Gregory B. Thompson[a,*], and Christopher R. Weinberger[b]
[a]*Department of Metallurgical and Materials Engineering, The University of Alabama, Tuscaloosa, AL 35487*
[b]*Mechanical Engineering and Mechanics Department, Drexel University, Philadelphia, PA 19104*
* Journal of the European Ceramic Society 35 (2015) 95-103

Abstract

For group VB transition metal carbides, as compared to group IVB carbides, an anomalous rise in hardness occurs for substoichiometric carbon concentrations as compared to the stoichiometric monocarbides. Here we report the computationally derived elastic constants, electronic density of states, and activation energies for carbon vacancy migration as a function of carbon content to elucidate their effect on the hardening responses. The changes in elastic properties with respect to carbon vacancy concentration show similar behaviors of elastic softening and decreasing hardness for all of the cubic carbides. The consistent trends of vacancy diffusion energy barriers between all of the group IVB and VB transition metal carbides also suggests that carbon diffusion may not be a significant contributor to the reported hardness differences. Consequently, we propose that the anomalous hardening for substoichiometric behavior is a competition between elastic constant softening and a microstructural-based effect, i.e. domain hardening, that is present in group VB carbides but not in group IVB carbides.

Introduction

The group IVB and VB transition metal carbides are a class of refractory ceramics that are well known for their thermal and structural stability. These materials form compounds that have the highest melting temperatures recorded and exhibit exceptional hardness, which are direct results of the mixed covalent-metallic-ionic bonding present in these compounds. Thus, they are well suited for structural applications at high temperatures where a variety of strengths are required.

At near equal parts transition metal and carbon, these materials typically form the rock salt or B1 structure. This structure is stable for a range of stoichiometry allowing a large amount of carbon loss. For the group VB compounds, the FCC structure of the metal atoms is maintained with the loss up to approximately 25% carbon at elevated temperatures. At lower temperatures, the carbon vacancies can order resulting the precipitation of a Me_6C_5 phase, where Me is the metal atom [1]. Further carbon loss may result in the precipitation of various faulted metal-rich carbide phases such as Me_4C_3 and Me_2C, which do not share the FCC metal sublattice ordering. Of the group VB metal carbides, vanadium carbide is unique. It does not form a stoichiometric B1 structure like TaC or NbC, rather it phase separates to substoichiometric VC_x and graphite, at carbon concentrations equal to or greater than X~0.88[2] . In contrast, the group IVB compounds can sustain much larger losses of carbon concentrations without the loss of the FCC metal sublattice. Thermodynamic and first principle calculations of these compounds have also shown the stability of equivalent vacancy ordered phases retaining the FCC metal lattice[3], but, to the

authors' knowledge, these phases have not been experimentally reported. None of the faulted metal-rich carbides are known to form in the group IVB carbides.

It is well known that vacancies can directly affect the thermal and structural stability and exert influence on mechanical properties of materials. Notably, the melting temperature of the group VB carbides has a maximum that is not located at stoichiometric MeC, but at some measurable carbon loss[1] . Additionally, the hardness measurements have also been reported to similarly trend with the peak hardness being sub-stoichiometric, Figure 1. For NbC_x and TaC_x this maximum is at C/Me=x≤0.85[4-7] . While various studies may not all show the same amount of hardening or the exact same carbon vacancy transitions, it is clear that such a substoichiometric transition occurs. In contrast, studies in the group IVB carbides have not shown a similar anomalous hardening and melting temperature behavior; in contrast, in each of these properties, the maximum property is at the stoichiometric C: Me ratio of equal parts [7] .

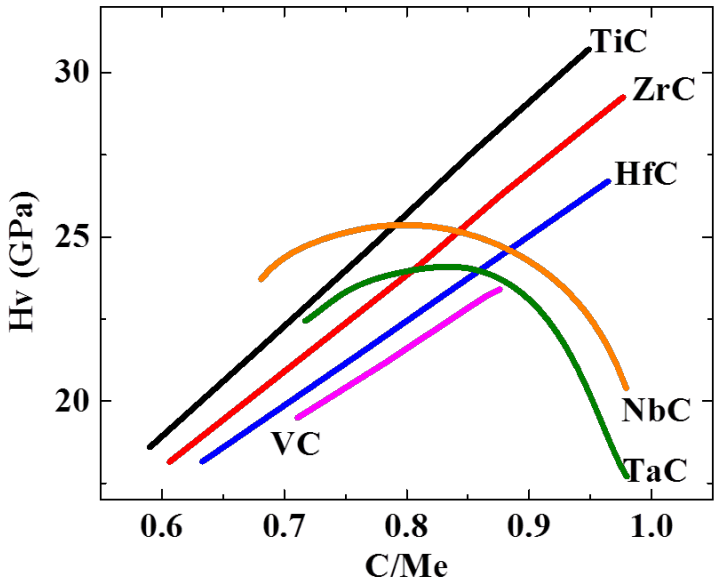

Figure 1: Representation of hardness as a function of transition metal carbide and carbon content. The image is a rendering of that reported in reference[4] .

Numerous theories have been developed to explain this difference in hardness between the group IVB and VB transition metal carbides, including optimal filling of the d-bands[4] , changes in slip systems[8-10] , as well as the potential hardening cause by substoichiometric phases[11] . The study by Jhi *et al*[12] supports, with electronic structure density functional theory (DFT) calculations, the notion that bonding has a direct effect on the hardness through the elastic constants. They showed that the shear modulus of NbC_x does not decrease nearly as much as TiN_x (which shows a comparable loss of hardness similar to TiC_x).Vacancies have also been postulated to control strength and plastic flow in these materials. These theories [7, 13-15] assume that carbon vacancy migration through the dislocation core is necessary for plastic flow at low and moderate

temperatures. Collectively, these prior results strongly suggest that the formation and migration of carbon vacancies in these materials is critical in understanding their properties and ultimately how to design these materials.

In this work, we investigate the properties of vacancies in all of the group IVB and VB transition metal carbides using electronic structure density functional pseudo-potential theory. We solely focus on the B1 structure with vacancies and compare our findings with available literatures. Notably, we compute the change in elastic properties with respect to carbon vacancy concentration for all of the cubic carbides. The comparison of these properties enables us to determine its contribution to the hardening/softening in indentation experiments. We also compute the vacancy formation energies as a function of the super-cell size, which allows us to compare the formation energy and stability across the cubic carbides. The computed vacancy migration energy in all of these materials will be compared against available experiments as well as predict some unmeasured properties. Finally, we examine how the densities of states in these materials change as a function of carbon content in the B1 structure. While numerous papers have computed elastic properties of the pure B1 structures[16-20], none have comprehensively computed the properties for a wide range of vacancy concentrations or materials. This self-contained approach will provide unique insight into the similarities and differences between the group IVB and VB cubic monocarbides and help to elucidate the anomalous hardening in group VB carbides that is not observed in group IVB carbides as shown in figure 1.

Methodology

To compute the energies used in estimating the vacancy formation energies, migration energies and elastic constants, we employed the electronic structure density functional theory as implemented in the Vienna Ab-Initio Simulation Package (VASP)[21, 22]. For all of our calculations, we use the Projector Augmented Wave (PAW) pseudo-potential[23, 24] and evaluate the exchange correlation energy using the Purdew-Burke-Ernzerhoff (PBE) formulation within the generalized gradient approximation (GGA)[25]. The energy cutoff used in all our calculations was 400 eV and integration in k-space was performed using Monkhorst-Pack with an integration that varied with simulation cell size[26].

In order to compute properties as a function of vacancy concentration, many different super-cell sizes were used. The primitive B1 unit cell consists of two atoms, but cannot support any vacancies without forming a pure substance. To resolve this issue, we used two types of super-cells: one that is based on an expanded form of the primitive cell and one that expanded upon the standard FCC unit cell. The primitive unit cell has two atoms and the expanded forms (equal in all directions) have 2, 16, 54, 128, ... $2*N^3$ atoms, where N is the number of atoms in the super-cell. The expanded FCC unit cells have 8, 64, 216, 512, ... $(2\ N)^3$ atoms. The 16 and 64 atom unit cells are shown in Figure 2 for reference. The advantage of using both of these types of super-cells is that removing a single vacancy (either carbon or metal) results in the super-cell retaining its cubic symmetry, even after relaxation, which allows us to simulate the formation of a relatively isolated vacancy as well as determine unambiguously the elastic constants for the sub-stoichiometric monocarbides.

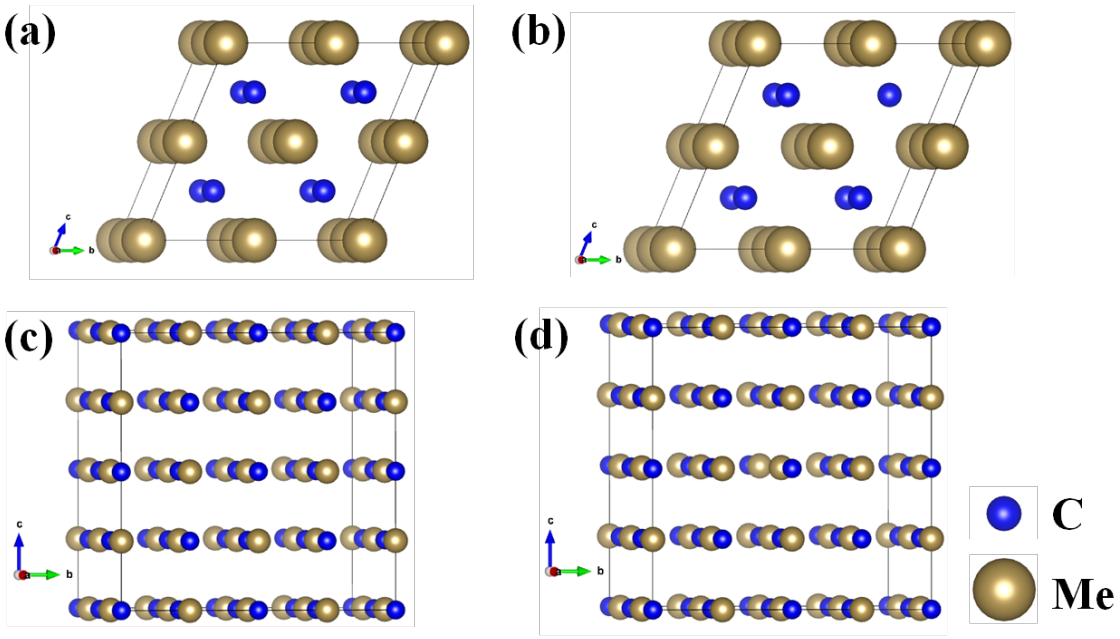

Figure 2: Schematic of the different unit cells of the cubic monocarbide to accommodate the carbon vacancies without the loss of the cubic symmetry **(a)** Perfect and **(b)** with a vacancy for the 16 atoms super-cell; **(c)** Perfect and **(d)** with a vacancy for 64 atoms super-cell.

Results and Discussion

Elastic constants

Most mechanical properties, i.e. strength and hardness, scale with elastic constants. We have computed both stoichiometric, Table 1, and substoichiometric, Table 2, elastic properties for each of the carbides. In addition, we have provided the lattice constant and cohesive energy for each of the stoichiometric B1 structures in Table 1. To evaluate the enthalpy of formation, the cohesive energies of the pure elements, metal and carbon atoms, were subtracted from the cohesive energy of the compound, with cohesive energies and lattice constants of the pure elements given in Appendix A for reference. We note that all of the compounds show positive enthalpies of formation and positive elastic constants

Table 1. Properties of the stoichiometric B1 monocarbides.

Property	TiC	ZrC	HfC	VC	NbC	TaC
a_0 (Å)	4.331	4.718	4.642	4.150	4.501	4.471
E_{coh} (eV/MeC)	14.71	15.83	16.26	14.01	15.71	17.23
ΔH_f (eV)	1.54	1.65	1.92	0.787	0.837	1.18
B (GPa)	270	238	253	332	302	340
C11 (GPa)	546	490	540	669	644	737
C12 (GPa)	133	112	112	152	129	141
C44 (GPa)	162	147	171	186	166	175

Table 2. The elastic constants of the B1 mono-carbides (in GPa).

Elastic Constant	TiC	ZrC	HfC	VC	NbC	TaC
X=0.75						
C_{11}	470	403	464	557	512	579
C_{12}	113	105	101	164	150	172
C_{44}	118	105	131	107	109	116
B	233	204	223	285	270	308
G	139	120	149	139	134	147
E	348	301	366	359	345	380
X=0.875						
C_{11}	520	460	508	640	608	684
C_{12}	117	104	107	138	126	147
C_{44}	154	139	162	170	153	157
B	252	223	223	305	287	337
G	171	153	176	199	181	195
E	419	374	425	490	452	488
X=0.96875						
C_{11}	541	484	535	663	628	709
C_{12}	127	108	110	143	133	147
C_{44}	162	146	170	184	162	169
B	265	234	252	317	287	337
G	179	161	184	211	192	207
E	438	394	445	518	474	515

To compute the elastic constants of the substoichiometric MeC_x compounds, three different super-cell sizes: 8, 16 and 64 atoms were used. The elastic constants for each of these super-cells had a single carbon vacancy, which led to values of x=0.75, 0.875 and 0.96875. The elastic constants of the 8 and 16 atom super-cells without vacancies were also computed for comparison and showed negligible variation from the values in Table 1. Though the extreme carbon loss can result in the precipitation or co-precipitation of metal-rich carbide phases, these simulation results provide the ability to clearly probe the trend in the B1 compounds' elastic constants with carbon loss, something that can be difficult to do experimentally. The cubic elastic constants are listed in Table 2 for all of the substoichiometric compounds.

The Hill average elastic constants, which are an average of the Voigt and Reuss elastic constants [27], given below, were determined from the computed cubic constants. This methodology allows the trends in elastic constants to be easily compared. The Voigt and Reuss shear modulus are defined by[28]

$$G_V = \frac{1}{5}(C_{11}\text{-}C_{12} + 3C_{44}) \qquad (1)$$

$$G_R = 5[4(S_{11}\text{-}S_{12}) + 3S_{44}]^{-1} \qquad (2)$$

And the Hill average shear modulus defined as

$$G = \frac{1}{2}(G_V + G_R) \qquad (3)$$

The Voigt and Reuss bulk modulus are the same as the bulk modulus of the cubic crystal, and hence so is the Hill bulk modulus. The other elastic constants can then be easily derived from the shear and bulk modulus.

The average shear modulus for all six cubic carbides are plotted in Figure 3 as a function of the carbon content. Figure 3(a) shows a direct comparison of the absolute average shear modulus value of all six compounds. Notably, the group VB carbides are stiffer than the group IVB carbides. Figure 3(b) is the same data normalized by the shear modulus at zero vacancy concentration. From this plot, it is obvious that all of the carbides appear to elastically soften with carbon vacancy concentration at the same rate. The only significant spread occurs at x=0.75, which may be a result of the high constraints on the atoms in these highly symmetric (and small) super cells.

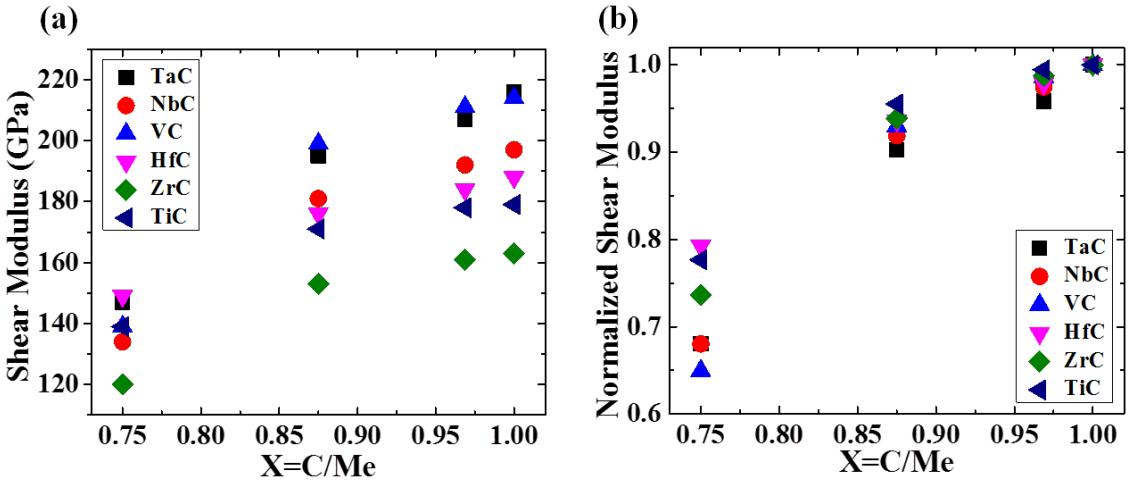

Figure 3: (a) Computed average shear modulus as a function of carbon content for the various transition metal carbides **(b)**The same shear modulus normalized by the shear modulus at x = 1.0.

The hardness for all the carbides was estimated using these computed elastic constants according to [29]

$$H_V = 2(k^2G)^{0.585}-3 \qquad (4)$$

where k is Pugh's modulus, which is the ratio of the shear modulus, G, and bulk modulus, B. These results are plotted in Figure 4. In general, the hardness increases with carbon content. The experimentally reported anomalous hardness peaks for substoichiometric TaC_x and NbC_x near $X\approx0.84$[4] was not captured in these simulations. This demonstrates that the anomalous hardness is not a direct consequence of the trends associated with the elastic constants.

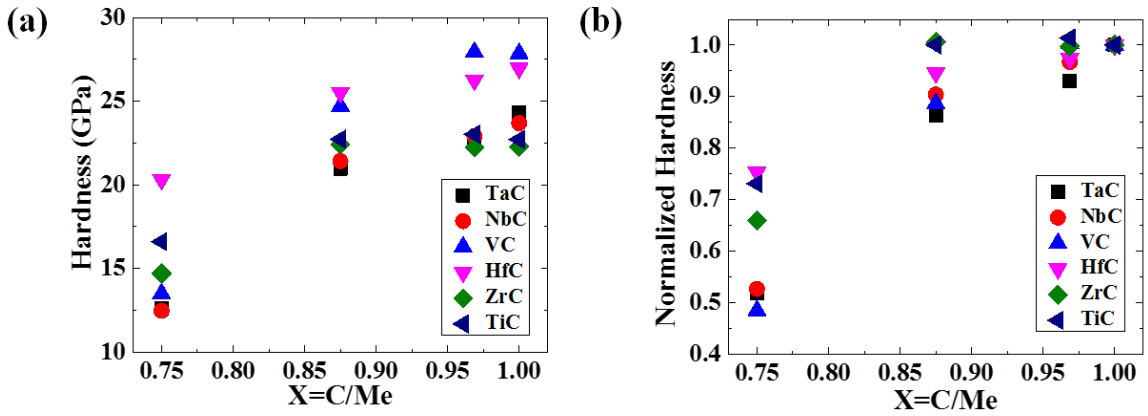

Figure 4: (a) The predicted hardness for each of the cubic carbides and **(b)** the same hardness normalized by the hardness at stoichiometry, i.e. x = 1.0.

Electronic Structure and Bonding

Some works have suggested that the bond structure of the carbides contributes directly to the anomalous hardness observed in TaC and NbC[4, 7]. The elastic constants computed above provide direct evidence to the contrary; all the transition metal carbides elastically soften at approximately the same rate with carbon loss. The electronic density of states (DOS) in the MeC, $MeC_{0.875}$ and $MeC_{0.75}$ structures for all of the cubic transition metal carbides has been computed. Examples of the total DOS computed for TaC (group VB carbide) and TiC (group IVB carbide) are shown in Figure 5. The DOS peak for TaC is near -5 eV, Figure 5(a), and is associated with the *pd* bonding between the tantalum and carbon atoms, which is covalent in nature. It appears that this peak decreases with vacancy concentration, signaling a decrease in the contribution from these bonds. Similarly, a slight increase in the DOS at the Fermi level accompanies this decrease which is interpreted as an increase in the *dd* bonding between the tantalum atoms. The TiC *pd* and *dd* bonding shows a similar trend, Figure 5(c), although the details, such as the peak location of the *pd* bonding (~-3 eV) is slightly different than that in TaC, Figure 5(a). These trends in the DOS with respect to carbon content are consistent between all of the other transition metal carbides. This transition from covalent towards metallic character results in a decrease in the strength of the bonds which is manifested in the elastic constants reported in Tables 1 and 2.

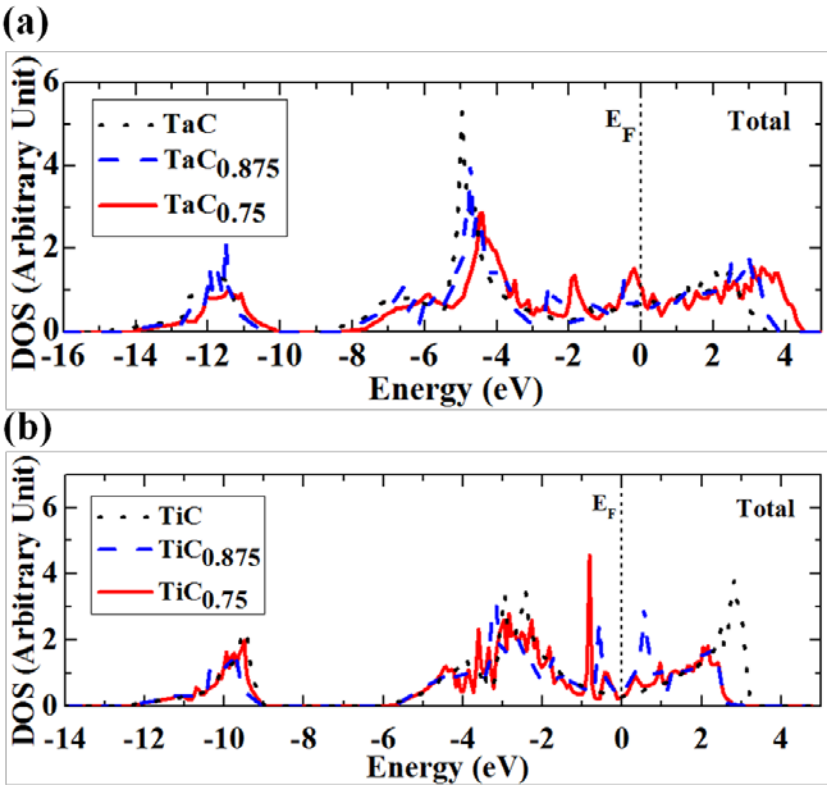

Figure 5: (a) The total density of states for TaC, $TaC_{0.875}$ and $TaC_{0.75}$. The DOS is normalized by the number of formula units. Alternatively, the normalization can be thought of as the number of metal atoms. **(b)** A comparative DOS plot of TiC.

Activation energies for diffusion.

Recognizing that carbon vacancy diffusion may contribute to plastic flow[14, 30-32], the anomalous peak in hardness may be associated with carbon diffusion. It has been proposed that carbon vacancy diffusion is the rate limiting step in plastic deformation. This is because the activation energy associated with plastic deformation is reported to be close to that of carbon vacancy diffusion[33].For example, at low temperatures, TaC is reported to slip on {111} planes [9, 34] and is this is same slip planes for most cubic carbides at elevated temperatures [8]. Slip on these close-packed planes is assisted by the dissociation of the perfect dislocation into partial dislocations[14, 35, 36]. This splitting motion can be aided if the carbon atoms diffuse through the dislocation core, or shear in a related fashion, such that metal atoms do not glide over other metal atoms, a plastic deformation mechanism termed the synchro-shear mechanism [15]. It is generally accepted that carbon diffusion is of particular importance to the deformation mechanics of these carbides.

Consequently, simulations were conducted on the formation energy and migration energy of carbon atoms for both carbide groups. Since carbon vacancies readily form in the transition metal carbides[1], this implies that the energy to form a carbon vacancy must be relatively low. Several studies using electronic structure theory have shown that the vacancy formation energies

are indeed low in TiC and NbC[37]. However, many of these calculations are done in relatively small super-cell volumes and wider comparisons between other group IVB and VB carbides have not been made. Here, we computed the energy to remove a carbon vacancy from a number of super-cell sizes that range between 4 and 108 metal atoms. The energy of the super-cell configuration with a single carbon vacancy is compared to a super-cell without a carbon vacancy to determine the energy to remove the carbon atom. To compute the vacancy formation energy, one must know the chemical potential of a carbon atom in the carbide. Given that a definitive measure of the chemical potential does not exist in this state, we have used the cohesive energy of a carbon atom in graphite. While this choice may not be ideal, it has provided substantial insight. If we define the vacancy formation energy in terms of the number of metal atoms, N, in the super-cell, the vacancy formation energy is given as:

$$E_v^f(MeC) = E(NMe, NC)\text{-}E(NMe, (N\text{-}1)C)\text{-}E(graphite) \quad (5)$$

and the super-cell size was increased until the energy converged. This converged value is an approximation to the vacancy formation energy in the stoichiometric monocarbide. As is pointed out by Tan et al. [37], we can also define an average vacancy formation energy in MeC_x as

$$\overline{E}_v^f\left(MeC_{x=(N\text{-}1)/N}\right) = E(NMe, NC)\text{-}E(NMe, (N\text{-}1)C)\text{-}E(graphite) \quad (6)$$

The vacancy formation energy for a metal atom is defined in a similar manner. However, in this case the chemical potential of the metal atom is taken as the cohesive energy of the pure metal.

The vacancy formation energy for both carbon and metal vacancies converge rapidly with cell size, as shown in the representative plot for hafnium carbide in Figure 6(a). This plot not only demonstrates the rapid convergence of the vacancy formation energy with the number of atoms in the super-cell but also highlights the asymmetry of the vacancy formation energies between the metal and carbon vacancies. Obviously, it is much easier to form an isolated carbon vacancy than a metal vacancy. Table 3 lists the converged carbon and metal vacancy formation energies for stoichiometry for each of the carbides.

Table 3: The formation energy (in eV) of the carbon and metal vacancies computed from the largest super-cell.

Material	Carbon Vacancy	Metal Vacancy
TiC	0.42	8.6
ZrC	0.28	9.4
HfC	1.1	9.3
VC	-0.93	4.5
NbC	-0.42	4.1
TaC	0.26	3.5

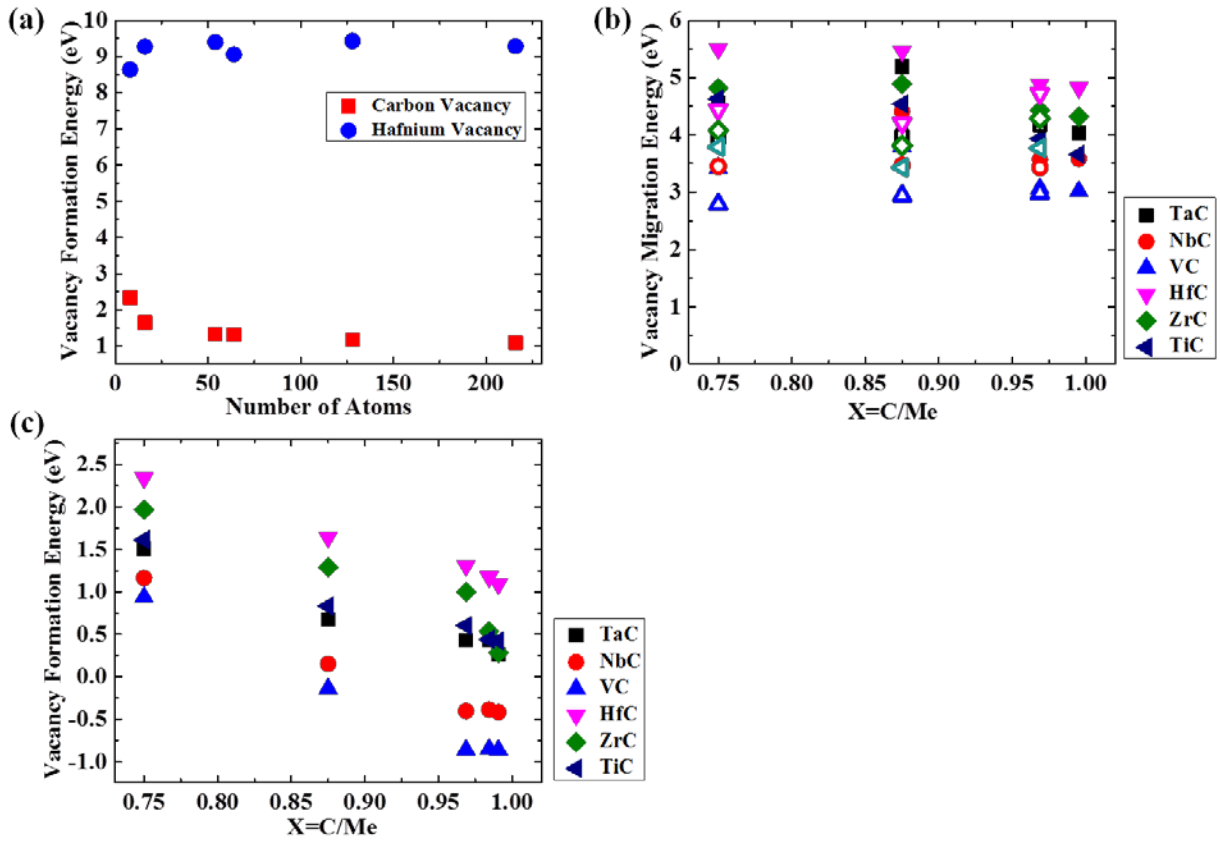

Figure 6: (a) The metal and carbon vacancy formation energy in hafnium carbide plotted as a function of the total atoms in the super-cell.**(b)**The average carbon vacancy formation for all of the compounds as a function of the carbon concentration.**(c)**The carbon vacancy migration energy plotted as a function of carbon content. The filled markers represent results from calculations with a rigid cell while the open markers are results where the cell is allowed to change shape and size.

The group IVB TiC, ZrC, and HfC as well as the group VB TaC all have positive carbon vacancy formation energies. This implies that the stoichiometric B1 phase is stable, as experimentally observed. The negative value for VC would indicate that the B1 phase is unstable or would spontaneously form vacancies. Recall, VC has not been reported to form the stoichiometric B1 phase[2] and these results would agree with experiments. In fact, most phase diagrams of vanadium carbide have shown the carbide separating between VC_x and graphite near X=0.88. Note that the average vacancy formation energy becomes positive around x=0.85, Figure 3(b).

The NbC was also noted to have a negative vacancy formation energy value, Table 3, yet is known to experimentally form the stoichiometric B1 phase[38]. The negative value arises because of the chemical potential used is the DFT computed cohesive energy of graphite, i.e. 7.85 eV/atom, and as noted previously would not be the chemical potential of carbon explicitly in these carbides. Consequently, this has affected the accuracy of some of the values reported. For the experimental cohesive energy of graphite, this difference is approximately ~0.45 eV[39] to the DFT computed

value; this discrepancy is commonly known to occur in DFT calculations for pure carbon. If the experimental value is used, the vacancy formation energy for NbC becomes essentially zero and the B1 phase is stable. Using the experimental cohesive energy value for graphite will shift all the computed vacancy formation energies up by 0.45eV in Table 3. Since we are consistently using DFT computed values throughout this work, we have chosen to retain those values here for consistency.

Coupling the computed vacancy formation energy with the migration energy, the activation energy for carbon vacancy diffusion can be now determined. The migration energy was computed assuming that the diffusion occurs along the <110> directions between metastable states for single carbon vacancies created above. The minimum energy path is determined using the nudged-elastic-band (NEB) method[40] to relax the initial path, which is a linear interpolation between the initial and final configuration. We used eleven discrete images in our calculation along this initial and final states with the migration energy determined for carbon contents of x=0.75, 0.675, 0.969, and 0.99. To determine the effects of constraints, the migration energy for fixed cell and flexible geometries were employed. For the fixed geometry, the super-cell is not allowed to change shape or size during NEB minimization while both are allowed to change for the flexible geometry. As one could expect, this geometry difference causes variations in the computed migration energies plotted in Figure 6(c), with the smaller cell geometries (or lower carbon concentrations) exhibited the most significant deviations. If the cell geometry is held fixed, the migration energies tended to decrease because the lower carbon concentrations have smaller lattice constants, hence bond distances, making migration more difficult. Interestingly, the lower migration energy of the flexible cells at lower carbon concentrations suggests that these cells may intrinsically be more flexible for the diffusion of atoms.

As a result of the migration energy spread in Figure 6(c), particularly at the lower carbon vacancy concentrations, it is not immediately obvious which value should be taken as the correct migration energy. This computational spread may provide insight into the experimental scatter reported for the activation energies in the various transition metal carbides, Table 4, because it may not have a fixed value. Since the computed values near stoichiometry are close to the mean of the values at higher carbon vacancy concentrations, these results do not support a concentration dependent migration energy. Therefore, we have assigned average migration energy to be the value near stoichiometry.

Table 4. The formation and migration energy (in eV) of the carbon vacancies and experimentally determined activation energies. The values in parenthesis in the experiments are the carbon concentration.

Material	E_v^f	E_v^m	Q	Experiments
TiC	0.42	3.7	4.1	4.13 (0.97) , 4.77 (0.67), 2.15 (0.67), 4.63 (0.89), 4.81 (0.47), 4.25 (0.87-0.96)[47-50]
ZrC	0.28	4.3	4.6	4.91 (0.92) ,4.94 (0.97)[51]
HfC	1.1	4.8	5.9	
VC	-0.93	3.0	3.0	2.91 (0.75), 3.11 (0.92), 3.69 (0.84)[51, 50]
NbC	-0.42	3.6	3.6	3.8 (0.7-0.93), 4.08-4.34 (0.75-0.97)
TaC	0.26	4.0	4.3	3.93 (0.99), 3.73 3.73, 4.3, 3.8[52 53]

Summing the migration and formation energy, the computed activation energy for diffusion is tabulated in Table 4. For NbC and VC, who's computed formation energies are negative, we have taken the formation energy in each of these two special cases to be zero. Considering the results in Table 4, there is no obvious difference in activation energies for diffusion that could contribute to plastic flow between the group IVB and VB transition metal carbides with respect to carbon concentration that would explain the anomalous hardness.

Phase and Microstructure

Considering those elastic constants, direct bonding, and vacancy properties are not direct causes of the anomalous hardening, an alternate explanation is necessary. The anomalous hardness is only reported to be near X~0.86[4, 7], which is near the composition for the Me_6C_5 phase. Of the transition metal carbides, this phase has only been experimentally reported only in the group VB carbides where the anomalous hardness is reported in the tantalum and niobium carbides. Any explanation that relates the anomalous hardness to the Me_6C_5 phase must account for its absence of a hardness peak in vanadium carbide. This can be accounted for considering that the phase and microstructures that form around these compositions.

In Figure 4, the computed hardness of the rock salt phase with vacancies demonstrates a universal decrease in hardness with carbon loss. In Figure 7, we have plotted the hardness associated with specific crystal structures that are associated with specific stoichiometries, i.e. Me_6C_5, Me_4C_3, etc. using prior reported elastic constants for those phases[3,41,44,45] . This plot, similar to Figure 4, reveals that the theoretical elastic constant derived hardness, equation (4), decreases with depleted carbon. Clearly, the formation of a specific metal-rich carbide phase also cannot directly explain the anomalous hardness. Rather, we believe the combination of phase and microstructure are necessary to elucidate this behavior, as only elastic constant contributions, not microstructure, are captured in the computed hardness values using equation (4).

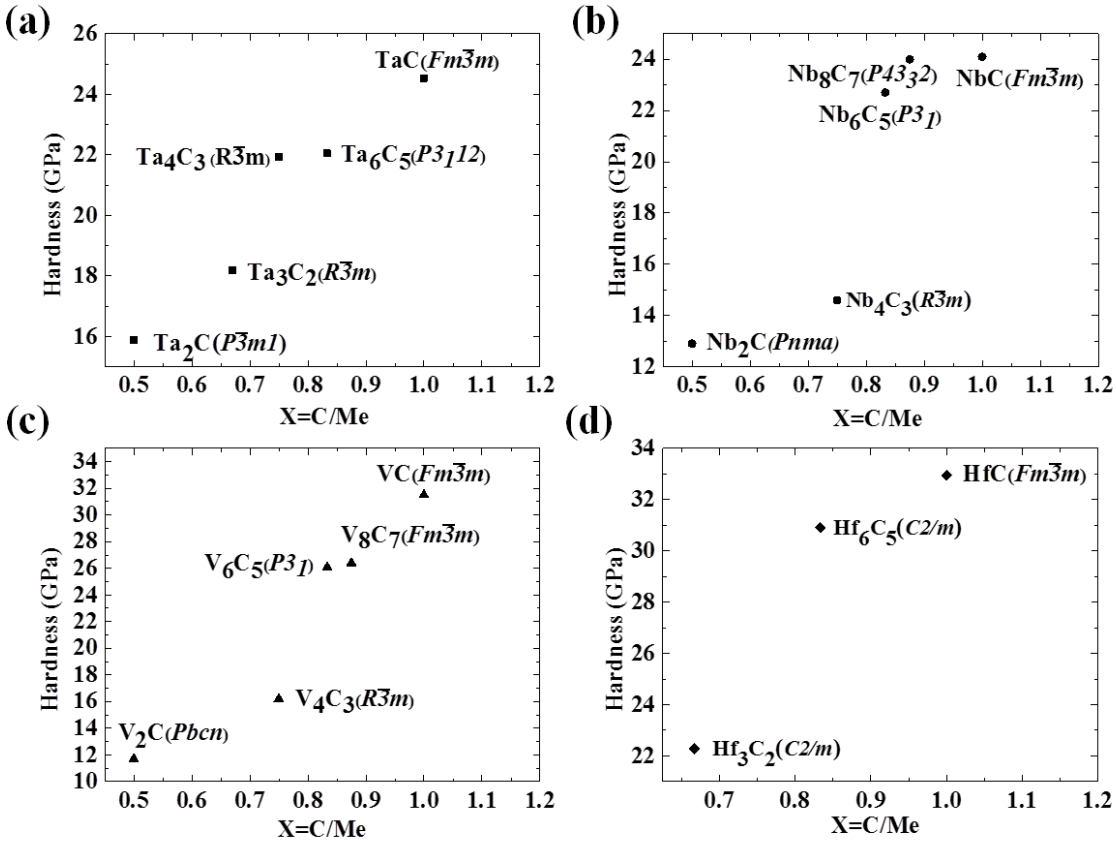

Figure 7: The predicted hardness from the elastic constants (reference given after each) for the specific phase present at that composition.**(a)**Tantalum carbides[44] **(b)** Niobium carbides[41] **(c)**Vanadium carbides[45] and **(d)** Hafnium carbides[3].

Following the ideas of Williams[42] and Morgan and Lewis[11], the peak in hardness is related to vacancy ordering in TaC_x and NbC_x[42]. Morgan and Lewis[11] argued that the rise in hardness in NbC_x occurs due to the superposition of two mechanisms: the hardening from domain boundaries in the ordered Nb_6C_5 phase and the increased Peierls stress due to the increase in cohesive energy of the ordered crystal. In their work, the isolated contributions of elastic constants and vacancy properties were not individually addressed, as done here, so that a firm conclusion of these contributions could not be eliminated as a possibility. Domain hardening in V_6C_5 has been reported to follow essentially a Hall-Patch relationship [43], which we expect to be true in other similar group VB tantalum and niobium carbides, though this experimental work has not yet been reported. Given that the Me_6C_5 phase is elastically softer than MeC, Figure 7, the combined microstructure of ordered domains within the host rock salt grains must be contributing to the anomalous increase in hardness. Considering our prior findings in section 3.1, the contribution from the cohesion of the solid must be a weak effect as the elastic constants continually decrease with a decrease in carbon content. Hence the dominant influence of the ordered Me_6C_5 phase must be significant in increasing the hardness in the microstructure via domain hardening.

The lack of anomalous hardness in vanadium carbide is not caused by a lack of domain hardening; contrary, it is the only carbide system of these groups that has experimentally demonstrated domain hardening [43]. But unlike the other carbides, this material is unable to thermodynamically stabilize the stoichiometric monocarbide, thus vanadium carbide has likely peaked its hardness at V_6C_5 but there is no other phase above this concentration to demonstrate the loss in hardness.

The lack of anomalous hardness in the group IVB carbides is contributed to the inability of these phases to precipitate out the vacancy ordered Me_6C_5 phase. The lack of this phase results in no opportunity for domain hardening; hence the hardness is solely dictated by the change in elastic constants.

Summary and Perspective

In this paper, the elastic constants, electronic density of states, and the activation energy for carbon vacancy migration have computed for the group IVB and VB carbides as a function of carbon content. The elastic constants showed a monotonic decrease with carbon loss. This translated to a decrease in covalent to more metallic type bonding. The relative constant values of the activation energy for diffusion with respect to carbon concentration suggest that carbon diffusion and its contribution to plastic flow and hardness cannot account for the observed anomalous hardness. The apparent correlation between the composition of the peak in the anomalous hardness and the Me_6C_5 phase strongly supports the idea that this phase is contributing to the anomalous hardness. This is strengthened by the fact that the anomalous hardness is only observed in materials that experimentally form this phase. However, our computational work demonstrates that the carbides should all elastically soften with carbon loss and that the anomalous hardness cannot solely be contributed to the elastic constants of this phase. Rather its precipitation as domains in the rock salt matrix grains provides for a microstructural hardening effect, i.e. domain hardening [(43)]. The computational study here has provided further insights that the cohesion of the solid is less significant in this contribution to hardness as previously speculated [4, 11, 12]. Thus, the anomalous hardness is a result of a competition between elastic constant softening and microstructure-based hardening mechanisms.

Acknowledgments

XX Yu and GB Thompson recognize Air Force Office of Scientific Research grant FA9550-12-1-0104, Dr. Ali Sayir program manager and the University of Alabama Office for Research Post-Doctoral Fellowship Program. Professor C.H. Turner of the University of Alabama and the Alabama SuperComputer (http://www.asc.edu/) are also acknowledged for access to their computational resources.

Appendix

Properties of the Pure Elements

The group IVB pure elements form a hexagonal close-packed structure and the group VB from body-centered cubic structures. The lattice constants and cohesive energies were computed

for these structures using the aforementioned DFT. The group VB elements were computed previously by the authors in a separate study but are reproduce here for convenience [46]. The cohesive energy and lattice constants for both graphite and diamond were computed as references for carbon. As noted in the main text, the cohesive energy for both graphite and diamond are about 0.4 eV too high. Also, the c lattice parameter of graphite is grossly incorrect as DFT has difficulty in capturing the out-of-plane sigma bonds. Both these deficiencies are well known.

Table A.1: Properties of the pure elements

Property	Ti	Zr	Hf	V	Nb	Ta	Graphite	Diamond
a (Å)	2.93	3.23	3.19	2.98	3.33	3.31	2.47	3.57
c (Å)	4.62	5.18	5.05				7.72	
E_{coh} (eV)	5.31	6.33	6.48	5.37	6.93	8.20	7.85	7.72

References

1. Gusev A. I. Disorder and order in strongly nonstoichiometric compounds: transition metal carbides, nitrides and oxides, Springer, 2001.
2. Lipatnikov V., Gusev A., Ettmayer P. & Lengauer W. Phase transformations in non-stoichiometric vanadium carbide. Journal of Physics: Condensed Matter 1999; 11: 163.
3. Zeng Q., Peng J., Oganov A. R., et al. Prediction of stable hafnium carbides: Stoichiometries, mechanical properties, and electronic structure. Physical Review B 2013;88: 214107.
4. Vinitskii I. Relation between the properties of monocarbides of groups IV–V transition metals and their carbon content. Powder Metallurgy and Metal Ceramics 1972; 11: 488-93.
5. Ramqvist L. Variation of hardness, resistivity, and lattice parameter with carbon content of group 5 b metal carbides. Jernkontorets Ann 1968; 152:465-75.
6. Ramqvist L. Variation of lattice parameter and hardness with carbon content of group 4 b metal carbides. Jernkontorets Ann 1968;152:517-23.
7. Holleck H. Material selection for hard coatings. Journal of Vacuum Science & Technology A 1986; 4:2661-9.
8. Rowcliffe D., Hollox G. Hardness anisotropy, deformation mechanisms and brittle-to-ductile transition in carbide. J. Mater. Sci. 1971; 6: 1270-6.
9. Rowcliffe D., Hollox G. Plastic flow and fracture of tantalum carbide and hafnium carbide at low temperatures. J. Mater. Sci. 1971; 6: 1261-9.
10. Lee D., Haggerty J. Plasticity and creep in single crystals of zirconium carbide. J Am Ceram Soc 1969;52: 641-7.
11. Morgan G., Lewis M. Hardness anisotropy in niobium carbide. J. Mater. Sci. 1974;9: 349-58.
12. Jhi S., Louie S. G., Cohen M. L. & Ihm J. Vacancy hardening and softening in transition metal carbides and nitrides. Phys. Rev. Lett. 2001; 86: 3348.
13. Hollox G. E. Microstructure and mechanical behavior of carbides. Materials Science and Engineering 1968; 3: 121-37.
14. Martin J., Lacour-Gayet P. , Costa P. Variation of Stress With Strain Rate and Temperature for TaC Between 1200 and 2200 C. Compt.rend. 1971; 272: 2127-30.
15. Lewis M., Billingham J. , Bell P. Nonstoichiometry in ceramic compounds., Univ. of Warwick, Coventry, Eng. 1973.
16. Chen W., Jiang J. Elastic properties and electronic structures of 4d-and 5d-transition metal mononitrides. J. Alloys Compounds 2010; 499: 243-54.

17. Li H., Zhang L., Zeng Q., et al. Structural, elastic and electronic properties of transition metal carbides TMC (TM= Ti, Zr, Hf and Ta) from first-principles calculations. Solid State Commun. 2011; 151: 602-6.
18. Wu Z., Chen X., Struzhkin V. V. Cohen R. E. Trends in elasticity and electronic structure of transition-metal nitrides and carbides from first principles. Physical Review B 2005;71: 214103.
19. Yang J., Gao F. First principles calculations of mechanical properties of cubic 5d transition metal monocarbides. Physica B: Condensed Matter 2012;407: 3527-34.
20. Jhi S., Ihm J., Louie S. G. , Cohen M. L. Electronic mechanism of hardness enhancement in transition-metal carbonitrides. Nature 1999;399:132-4.
21. Kresse G., Hafner J. Ab initio molecular dynamics for liquid metals. Physical Review B 1993;47: 558.
22. Kresse G., Furthmüller J. Efficient iterative schemes for ab initio total-energy calculations using a plane-wave basis set. Physical Review B 1996;54:11169.
23. Blöchl P. E. Projector augmented-wave method. Physical Review B 1994; 50: 17953.
24. Kresse G., Joubert D. From ultrasoft pseudopotentials to the projector augmented-wave method. Physical Review B 1999; 59:1758.
25. Perdew J. P., Burke K. , Ernzerhof M. Generalized gradient approximation made simple. Phys. Rev. Lett. 1996;77:3865.
26. Monkhorst H. J., Pack J. D. Special points for Brillouin-zone integrations. Physical Review B 1976; 13: 5188-92.
27. Hill R. Elastic properties of reinforced solids: some theoretical principles. J. Mech. Phys. Solids 1963; 11: 357-72.
28. Hill R. The elastic behaviour of a crystalline aggregate. Proceedings of the Physical Society.Section A 1952; 65: 349.
29. Chen X., Niu H., Li D. , Li Y. Modeling hardness of polycrystalline materials and bulk metallic glasses. Intermetallics 2011; 19: 1275-81.
30. Rowcliffe D. J. Plastic deformation of transition metal carbides. In Deformation of Ceramic Materials II, ed. Anonymous Springer 1984 : 49-71.
31. Kumashiro Y., Nagai Y., Katō H., Sakuma E., Watanabe K. & Misawa S. The preparation and characteristics of ZrC and TaC single crystals using an rf floating-zone process. J. Mater. Sci. 1981; 16: 2930-3.
32. Kumashiro Y., Nagai Y. , Katō H. The Vickers micro-hardness of NbC, ZrC and TaC single crystals up to 1500 C. J. Mater. Sci. Lett. 1982; 1: 49-52.
33. Thompson G., Weinberger C. Tantalum Carbides: Their Microstructures and Deformation Behavior. Ultra-High Temperature Ceramics: Materials for Extreme Environment Applications, 2014,
34. Kim C., Gottstein G. , Grummon D. Plastic flow and dislocation structures in tantalum carbide: Deformation at low and intermediate homologous temperatures. Acta metallurgica et materialia 1994; 42: 2291-301.
35. Lewis M., Billingham J. , Bell P. Nonstoichiometry in ceramic compounds. Univ. of Warwick, Coventry, Eng. 1973.
36. Kelly A., Rowcliffe D. Slip in titanium carbide. physica status solidi (b) 1966; 14:K29-33.
37. Tan K., Bratkovsky A., Harris R., et al. Carbon vacancies in titanium carbide. Modell Simul Mater Sci Eng 1997;5:187.
38. Gusev A. I. Order–disorder transformations and phase equilibria in strongly nonstoichiometric compounds. Physics-Uspekhi 2000; 43:1.

39. Kittel C. Introduce to Solid State Physics. Wiley, New York, 1996.
40. Henkelman G., Uberuaga B. P. & Jónsson H. A climbing image nudged elastic band method for finding saddle points and minimum energy paths. J. Chem. Phys. 2000;113: 9901-4.
41. Wu L., Wang Y., Yan Z., Zhang J., Xiao F. & Liao B. The phase stability and mechanical properties of Nb-C system: using first-principles calculations and nano-indentation. J. Alloys Compounds 2013; 561: 220–227.
42. Williams W. S. Transition-metal carbides. Progress in Solid State Chemistry 1971; 6: 57-118.
43. Hannink R., Murray M. The effect of domain size on the hardness of ordered $VC_{0.84}$. Acta Metallurgica 1972; 20:123-31.
44. Yu X., Weinberger C. R. & Thompson G. B. *Ab Initio* Investigations of the Phase Stability in Tantalum Carbides. Submitted to Acta Materialia.
45. Wu L., Yao T., Wang Y., Zhang J., Xiao F. , Liao B. Understanding the mechanical properties of vanadium carbides: Nano-indentation measurement and first-principles calculations. J. Alloys Compounds 2012; 548: 60–64.
46. Weinberger C. R., Tucker G. J. & Foiles S. M. Peierls potential of screw dislocations in bcc transition metals: Predictions from density functional theory. Physical Review B 2013; 87:054114.
47. Sarian S. Diffusion of carbon in TiC. J. Appl. Phys. 2003;39:3305-3310.
48. Sarian S. Anomalous diffusion of 14C in TiC0. 67. J. Appl. Phys. 2003; 39:5036-5041.
49. Kohlstedt D., Williams W. S. & Woodhouse J. Chemical diffusion in titanium carbide crystals. J. Appl. Phys. 2003; 41:4476-4484.
50. Eremeev V., Panov A. Porosh. Met. 1967; 7: 65.
51. Sarian S. Carbon self-diffusion in disordered V_6C_5. Journal of Physics and Chemistry of Solids, 1972, 33:1637-1643.
52. Brizes W. F., Cadoff L. , Tobin J. Carbon diffusion in the carbides of niobium. J. Nucl. Mater., 1966, 20: 57-67.
53. Resnick R., Steinitz R. , Seigle L. Determination of diffusivity of carbon in tantalum and columbium carbides by layer-growth measurements. Trans. Met. Soc. AIME, 1965:233.

3. *Ab Initio* Investigations of the Phase Stability in Tantalum Carbides

Xiao-Xiang Yu[a], Christopher R. Weinberger[b], Gregory B. Thompson[a,*]
[a]*Department of Metallurgical and Materials Engineering, The University of Alabama, Tuscaloosa, AL 35487*
[b]*Mechanical Engineering and Mechanics Department, Drexel University, Philadelphia, PA 19104*

* Acta Materialia 80 (2014) 341-349

Abstract

Using a variable-composition *ab initio* evolutionary algorithm, the stability of various tantalum carbide compounds at ambient pressure and at 0K was investigated. The results revealed that TaC, Ta_6C_5 and Ta_2C are the lowest energy configurations with Ta_4C_3 and Ta_3C_2 having slightly higher energies. The vacancy ordered Ta_6C_5phase had three energetically degenerate structures. A competition between vacancy ordered and stacking fault variation of the phases was seen, with the latter becoming more favorable with lower carbon content. The close formation enthalpy of each stable and metastable phase appears to 'frustrate' the carbide in the co-precipitation of multiple phases for substoichiometric compositions. Density functional theory calculations also provided the elastic constants for each of the stable and metastable phases. As the carbon content increased, the elastic constants values increased. This has been associated with the change in metallic to more covalent bonding of the carbide from the density of states. The collective results of this computational work provide insight into why specific tantalum carbide phases form and the consequences they have on microstructure and properties.

Introduction

Tantalum carbides, along with others in the group VB transition metal carbides, exhibit a range of high to ultrahigh melting temperatures, microstructures controlled by the co-precipitation of metal-rich carbide phases, and varied mechanical behaviors dependent on the phase content [1,2,3,4,5,6]. Consequently, these materials have been proposed for various thermal heat protection, automotive wear resistant liners, and other types of thermo-mechanical loading applications [7,8,9]. Though these carbides maybe classified as ceramics, which are often considered to be hard and brittle materials, some tantalum carbide phases exhibiting significant plasticity that exceeds 30% at elevated temperatures [3,10]. Thus, the potential exists in this system to create multiphase carbides that exhibit varied mechanical properties, which provides unique opportunities to tailor their microstructure-mechanical property relationships. For example, it has been reported that a high volume fraction of Ta_4C_3 within a tantalum carbide matrix increases the room temperature K_{IC} to ~12-14 MPa$\sqrt{m}$ [10,11], though the associated toughening mechanisms for this increase have not been fully elucidated but is likely linked to the material's microstructure. These high fracture toughness microstructures consist of several co-precipitated nanoscale Ta_4C_3 laths, which are believed to contribute to extrinsic toughening. The precipitation and orientation relationship of the Ta_4C_3 phase is dictated by the close packed planes and directions of the parent material [1,12,13]. If the parent phase is TaC, with four {111} close-packed plane variants, a crisscross pattern of Ta_4C_3 laths forms in an equiaxed grain structure, figure 1(a). In contrast, precipitation of Ta_4C_3 from a parent Ta_2C phase results in parallel lath formation because of Ta_2C's

single close packed basal plane [2], figure 1(b). These grains also appear to be more acicular [2]. Unlike the group VB metal carbides, the group IVB metal carbides do not form these metal-rich phases [14] limiting the opportunities to tailor the microstructure, hence mechanical properties, through phase transformation routes. By understanding the phase equilibrium of the group VB metal carbides insights can be gained that are is crucial in tuning the microstructures and mechanical properties of these unique materials.

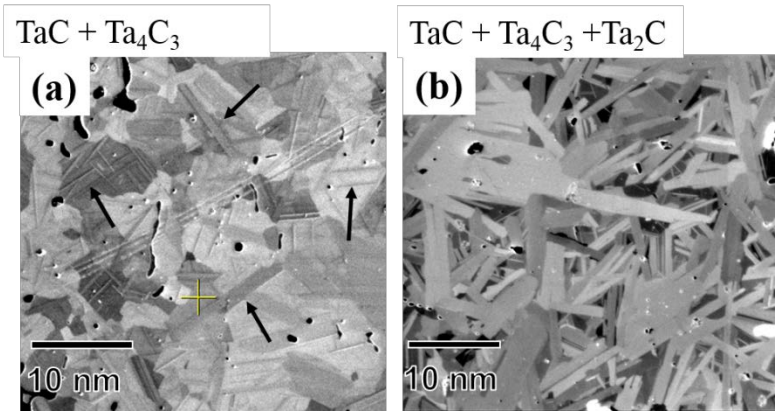

FIGURE 1: (a) Micrograph of TaC_x with crisscross laths of Ta_4C_3 (pointed to by arrows) for a 55Ta:45C sample. (b) Micrograph of TaC_x + Ta_4C_3 + Ta_2C for a 63Ta:37C sample. The x-ray diffraction of these phases with these microstructures can be found in reference [1].

In this paper, we explore the stability and structure of the tantalum carbide phase diagram using electronic structure density functional theory calculations. To date, there has not been a comprehensive and inclusive computational investigation of the different phases that comprise the tantalum carbon system [15]. In contrast, there has been some limited computational investigations into the group VB niobium and vanadium carbides [16,17]. According to the phase diagram of the Ta-C system provided by Gusev *et al*. [18,19], there are four compounds in the tantalum rich portion of the diagram: TaC, Ta_6C_5, Ta_4C_3 and Ta_2C. The structure, space group, and lattice parameter for these phases are tabulated in Table I. The monocarbide phase of TaC forms the B1 or rock salt crystal structure and similar to other group VB metal carbides is not a line compound. It can accommodate the loss of some carbon creating several site-occupancy defects [20] with an accompanying change in lattice parameter [18]. For substoichiometric TaC_{1-x} at temperatures lower than approximately 1500 K, a Ta_6C_5 phase can precipitate. This phase's experimental presence is very uncommon and has been suggested to require a very low cooling rate (~0.15 K/minute) to form [19]. Consequently, it is not even shown on the Ta-C phase diagram by Fisk [21]. Gusev *et al*. [14,18] proposed that this phase is derived from cubic TaC_{1-x} where the vacancies create a vacancy ordered structure that is either monoclinic or trigonal. Unlike the tantalum carbides, this Me_6C_5 phase (where Me is a metal) is more frequently observed in the niobium and vanadium carbides [18], which are also group VB metal carbides. The phase stability between the sub-stoichiometric TaC_{1-x} structure and these yet to be definitively determined Ta_6C_5 structures provides clear motivation for further computational investigation.

Unlike the Ta_6C_5 phase, the rhombohedral ζ-Ta_4C_3 phase has been experimentally observed by several groups [19],[22],[23,24]. Similar to the Ta_6C_5 phase, there has been some debate on its

thermodynamic stability. In the pioneering work of Rudy and Harmon [12], they noted that the Ta_4C_3 phase formed under compressive stresses by epitaxially growing off of the TaC_{1-x} phase when the temperature was too low to phase transform directly into Ta_2C. After 400 hours at 1700ºC, Ta_4C_3 decomposed suggesting to them that Ta_4C_3 phase was metastable. Considering this phase's significant effect on tantalum carbide's mechanical behavior as noted above [11], understanding its thermodynamic stability is essential. This phase has also been shown to experimentally co-exist in the presence of TaC and Ta_2C; yet thermodynamics dictates that only two phases should exist in binary systems providing yet further need to elucidate the phase equilibrium between all of these phases.

Further reduction in carbon will stabilize the Ta_2C phase where the metal atoms form a hexagonal closed-packed arrangement. This stoichiometric ratio compound exhibits an order - disorder transition with temperature. At temperatures less than ~1800 K, the α-Ta_2C's carbon sublattice is ordered, occupying every other plane of octahedral interstices, while at elevated temperatures this sublattice disorders [25]. Further loss in carbon does not result in any additional carbide compounds. The metallic body centered cubic Ta phase exhibits negligible carbon solubility except at temperature near 3000 K [19].

Tantalum carbides represent a rich collection of phases where the stability and microstructure are still not completely understood. The clear links of phase content with microstructure formations and mechanical properties dictates the need for a definitive equilibrium investigation. This work aims to clarify the energetics associated within the tantalum carbide compounds to better understand their intrinsic stability.

Computational methodology

The stoichiometric compounds and their crystal structures were predicted by using the evolutionary algorithm implemented in the USPEX code [26, 27].This approach features global optimization with real-space representation and flexible physically motivated variation operators. For each candidate structure generated by USPEX, the density functional theory (DFT) calculations were performed at 0K by application of the Vienna Ab-initio Simulation Package (VASP) [28, 29]. The compounds in the Ta-C system explored in this work contained up to 30 atoms in the unit cell. The initial generation consisted of 50 structures produced randomly. All the subsequent generations contained 40 structures, of these, 40% of the new structures were produced by heredity, 20% produced by soft mutation, another 20% produced by transmutation, and the final 20% produced randomly. Thermodynamically stable structures were determined by a convex hull construction; a phase was stable if its decomposition enthalpy into any other structures was positive [30]. The calculation was terminated when the stable structures did not change for 10 generations. The VASP simulations utilized the projector augmented wave method [31,32] in conjunction with the generalized gradient approximation (GGA) using the parameterization by Perdew, Burke and Ernzerhof (PBE) [33]. Plane waves with a cutoff energy of 600 eV and k-point mesh resolution in reciprocal space of $2\pi\times0.03$ $Å^{-1}$ yielded converged results. Denser k-point meshes in reciprocal space, with a resolution of $2\pi\times0.02Å^{-1}$ were employed for the elastic constants and density of states (DOS) calculations. The phonon spectra were obtained by Phonopy code [34] using the force constants calculated by VASP.

Results and discussions

Thermal stability of various compounds

The enthalpies of formation for each of the compounds identified are shown in figure 2(a), while the stable compounds are highlighted in black and tabulated in Table I and II. The thermodynamically stable phases were found to be TaC ($Fm\bar{3}m$), Ta_6C_5 (C2/m) and Ta_2C ($P\bar{3}m1$). Since TaC and Ta_2C are commonly observed in the literature, these results were not unexpected. In contrast, the stability of Ta_6C_5 could be considered, by some, a surprise. No imaginary phonon frequencies were found throughout Ta_6C_5's Brillouin zone's phonon dispersion curves, figure 2, suggesting dynamical stability. For comparison, the formation enthalpies of the two proposed Ta_6C_5 structures (C2 and $P3_1$) by Gusev [14] were also calculated and tabulated in Table I and II. Their phonon spectrums also were found not to have any imaginary frequency and are also plotted figure 3. Interestingly, these results demonstrate that these Ta_6C_5 phases cannot be distinguished energetically by DFT calculations, which means they are degenerate. The consequences of this will be further developed in the proceeding discussion. The prior C2 and $P3_1$ structures were assumed to have vacancies in perfect sites; however, after structural relaxation, the structures changed slightly. The C2 structure became C2/c (15) and the $P3_1$change to $P3_112$ (151).

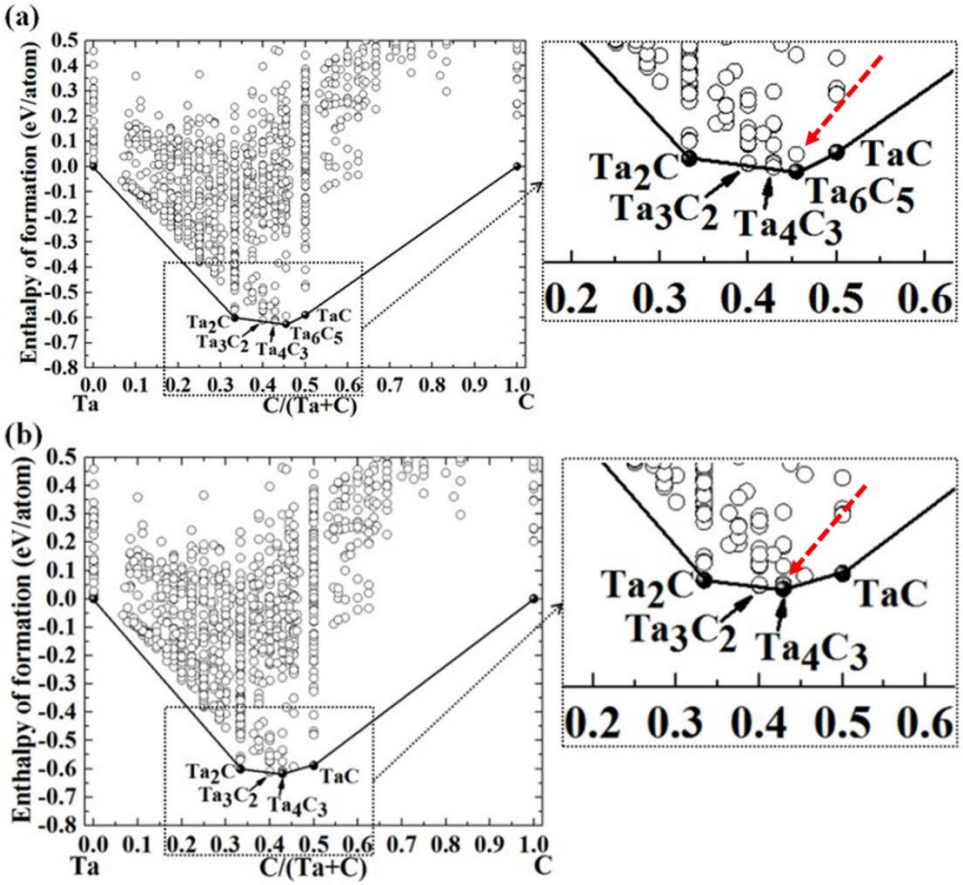

FIGURE 2. (a) The convex hull construction of the Ta-C system at ambient pressure. Circles denote different structures; those filled circles located on the convex hull are thermodynamically stable and are labeled in the image; the open circles represent structures with higher energy. The dashed arrow in the enlarged image points to the fault-formed Ta_6C_5 phase which is at a slightly

higher energy than the vacancy formed Ta_6C_5 filled circle (b) The convex hull construction of the Ta-C system without Ta_6C_5. The Ta_4C_3 phase, commonly observed in experiments, being identified as the next lowest energy structure for substoichiometric TaC_x to decompose into. The dashed arrow in the enlarged image points to a vacancy ordered Ta_4C_3 phase that is at a slightly higher energy than the fault-formed Ta_4C_3 phase that is now in contact with the convex hull boundary.

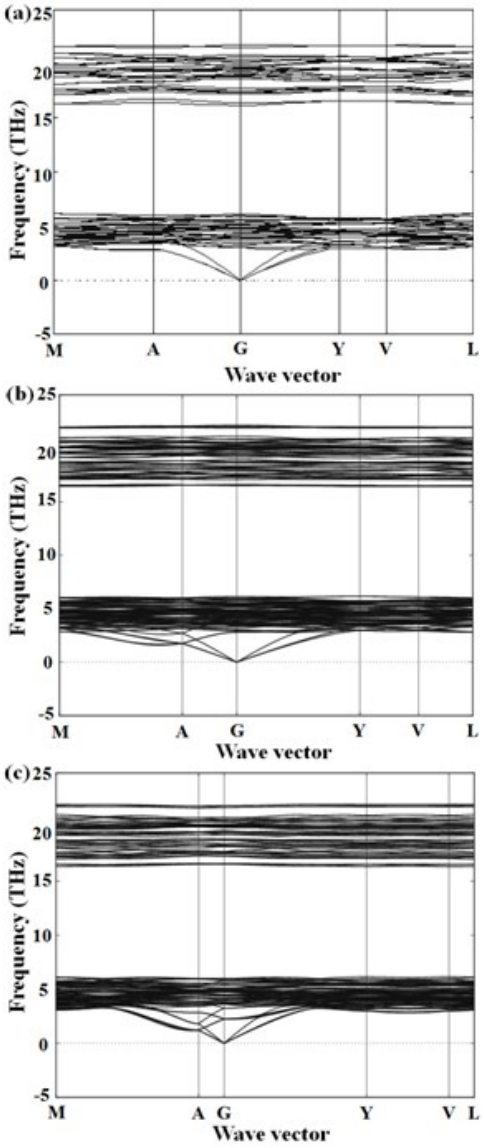

FIGURE 3. Phonon dispersion curves of Ta_6C_5: (a) C2/m (b) C2/c (c) $P3_112$.

Table I. The crystallographic data of stable and meta-stable tantalum carbides.

Compound	Space group	Lattice constants (Å) This work	Experimental results	Atom positions (Wyckoff position)
TaC	$Fm\bar{3}m$	a=4.47	a=4.46[41]	Ta(4a) (0.0,0.0,0.0) C(4b) (0.5,0.5,0.5)
Ta_6C_5	C2/m	a= 5.46 b= 9.47 c= 5.45 β=109.67°		Ta(8j) (0.24358,0.17417,0.24757) Ta(4i) (0.76074,0.00000,0.23907) C(4g) (0.00000,0.66677,0.00000) C(4h) (0.00000,0.16436,0.50000) C(2a) (0.00000,0.00000,0.00000)
	C2/c	a= 5.47 b= 9.47 c= 10.89 β=109.41°		Ta(8f) (0.75926, 0.00744, 0.8758) Ta(8f) (0.73514, 0.33269, 0.8761) Ta(8f) (0.26227, 0.15857 , 0.8814) C(4e) (0.0, 0.33354 , 0.25) C(4e) (0.0, 0.998 , 0.25) C(4b) (0.0, 0.5 , 0.0) C(8f) (0.5, 0.333 , 0.0)
	$P3_112$	a= 5.46 b= 5.46 c= 15.42 γ=120.0°		Ta(6c) (0.11207,0.20788, 0.41580) Ta(6c) (0.45943, -0.0944, 0.41253) Ta(6c) (0.76274, 0.55730,0.41613) C(3b) (0.77775, 0.22225, 0.83333) C(3b) (0.11333, 0.88667, 0.83333) C(3a) (0.11062, 0.88938, 0.33333) C(3a) (0.44351, 0.55649, 0.33333) C(3a) (0.77745, 0.22255, 0.33333)
	$R\bar{3}m$	a=3.15 b= 3.15 c=45.84 γ=120.0°		Ta(6c) (0.000, 0.000,0.58530) Ta(6c) (0.000, 0.000,0.30647) Ta(6c) (0.000, 0.000,0.13907) C(6c) (0.000, 0.000, -0.05305) C(6c) (0.000, 0.000, 0.77664) C(3b) (0.000, 0.000, 0.50000)
Ta_4C_3	$R\bar{3}m$	a=3.14 b= 3.14 c= 30.39 γ=120.0°	a=3.12, c= 30.06 [19]	Ta(6c) (0.000, 0.000, 0.78952) Ta(6c) (0.000, 0.000, 0.62592) C(3b) (0.000, 0.000, 0.50000) C(6c) (0.000, 0.000, 0.08036)
	C2/c	a= 6.23 b= 12.56 c= 5.45 β=124.86°		Ta(8f) (0.24822, 0.19059, 0.75122) Ta(8f) (0.23955, 0.06458, 0.23260) C(4e) (0.000, 0.18464, 0.2500) C(4e) (0.000, -0.06186, 0.2500) C(4e) (0.000, 0.68900, 0.2500)
Ta_3C_2	$R\bar{3}m$	a=3.14 b= 3.14 c= 22.45 γ=120.0°		Ta(3a) (0.000, 0.000, 0.00000) Ta(6c) (0.000, 0.000, 0.22069) C(6c) (0.000, 0.000, 0.60798)
Ta_2C	$P\bar{3}m1$	a=3.11, b=3.11 c= 4.95 γ=120.0°	a=3.10, c= 4.94[42]	Ta(12j) (0.333,0.667,0.753) C(6h) (0.0,0.0,0.5)

Table II. The formation enthalpies of the stable and meta-stable tantalum carbides.

Compound	Space group	Enthalpy of formation (eV/atom)
TaC	$Fm\bar{3}m$	-0.59
Ta_6C_5	C2/m	-0.63
	C2/c	-0.63
	$P3_112$	-0.63
	$R\bar{3}m$	-0.59
Ta_4C_3	$R\bar{3}m$	-0.62
	C2/c	-0.61
Ta_3C_2	$R\bar{3}m$	-0.61
Ta_2C	$P\bar{3}m1$	-0.60

As mentioned by Gusev [14], these superstructures have identical short-range order and are similar up to the third coordination sphere with respect to the metal atom. Consequently, they have nearly equal formation energies as proven by this work. Unlike the niobium and vanadium carbides, where the Me_6C_5 phase is observed more frequently in experiments [18], the lack of consistent identification of this phase in the tantalum carbides could be attributed to several (potentially compounding) factors. First, as noted by Gusev [19] and alluded to above, this phase appears to require very slow cooling rates in order for vacancy ordering to occur. These cooling rates are impractical in most high temperature fabrication processing resulting in the higher temperature rocksalt TaC_{1-x} to be quenched-in at room temperature. Second, the vacancy migration energies (formation + diffusion) within the tantalum carbides (~4.3 eV) are higher than either the niobium carbides (~3.6 eV) and vanadium carbides (~3.0 eV) [35], where these phases are more readily observed. These computed vacancy formation energies were found from the energy needed to extract a carbon atom from the B1 metal carbide structure; the migration energy was computed from the minimum energy path determined using the nudged-elastic-band (NEB) method. This higher energy barrier would potentially further hinder phase transformations, which occurs through long-range vacancy ordering. Supporting this idea is the experimental observations in niobium and vanadium carbides that Me_6C_5 forms as domains within the monocarbide rather than consuming the full grain [36]. Third, the indistinguishable enthalpies of formation of the Ta_6C_5 structures, Table II, suggest that multiple types of long range ordering may occur, which would make it difficult to identify a specific Ta_6C_5 structure. Finally, the larger scattering ratio of tantalum-to-carbon, in comparison to other group VB transition metal carbides, and similar electron diffraction patterns further inhibits clear identification and classification of the Me_6C_5 phase in the tantalum carbon system.

The second lowest energy Ta_6C_5 structure found by USPEX is the $R\bar{3}m$ phase, also tabulated in Table I and II. It's location on the convex hull plot of figure 2(a) is indicated by the dashed arrow. This is a 'faulted structure' similar to the Ta_4C_3 phase that will be further discussed below. The formation enthalpy of this phase is ΔE ~0.04 eV/atom higher than those of the vacancy ordered forms. Considering that this calculation was done at 0K, this small energy difference can be easily overcome with increasing temperature by the vibration contributions to the free energy of formation. Though vacancy ordered phases have slightly lower formation enthalpies, the kinetic

process of ordering also makes them possibly more difficult to occur. In contrast, the faulted structure is potentially more likely because the fault formation process requires vacancy condensation to one particular plane, a localized effect, which would be followed by shear associated with Shockley dislocations to create the fault [13]. The true formation of this faulted Ta_6C_5 phase would then require the appropriate number and spacing of these types of faults. In addition, the competition between the 'faulted' structure and the vacancy ordered forms is further complicated by kinetic processes.

Besides the aforementioned stable compounds, Ta_4C_3 ($R\bar{3}m$) and Ta_3C_2($R\bar{3}m$) were found to be very close to the convex hull curve, figure 2(a), and whose enthalpies of formation are slightly higher than the thermodynamic stable phases, Table II. Recognizing that the Ta_6C_5 phase is not commonly observed experimentally, it has been removed and a 'metastable' convex hull boundary is re-plotted in figure 2(b). In this case, the Ta_4C_3, along with TaC and Ta_2C, are on the convex hull with Ta_3C_2 at a slightly higher energy. The slightly higher energy of Ta_3C_2 may explain why this phase, as compared to Ta_4C_3, has not been reported experimentally.

These metal-rich carbide fault-formed structures ($R\bar{3}m$) can be created from the B1 TaC structure by the removal of specific {111} carbon layers. This carbon removal would then place metal-metal Ta {111} planes into contact. A subsequent shear on this metal-metal contact plane created by Shockley partial dislocations would then create the requisite stacking fault. The conventional trigonal unit cell for each of these phases must contain 3 faults to match the stacking sequence of the parent TaC phase. This results in there being 3 times as many metal planes in the stacking sequence as are required for stoichiometry for this phase. Specifically, there are 12 metal layers in Ta_4C_3, 9 in Ta_3C_2 and 18 in Ta_6C_5as shown in Table III. The resulting stacking sequence of Ta_3C_2 is A γ B α C | B α C β A | C β A γ B where A,B and C denote the stacking of the Ta atoms; α, β and γ denote the stacking of the carbon atoms; and | denotes a removal of a carbon plane and creation of the stacking fault. This fault-based formation mechanism proposed by Rowcliff [13] provides the removal of the carbon for the local composition change with the shear necessary for the crystallographic change that creates the new phase. It is worth pointing out that Ta_2C follows this carbon removal strategy but only has two metal atoms in the trigonal unit cell and belongs to a different space group, $P\bar{3}m1$; this is because of its unique stacking. The model given above collapses into the higher symmetry $P\bar{3}m1$ class though they share the same point group $\bar{3}$.

The ordered removal of a carbon plane, or alternatively the ordering of vacancies on a plane, is similar to experimental observations of Frank loops in face centered cubic metals [37] or the precipitation mechanisms of γ' in α in Al-Ag alloys [38]. Wang et al. [39] recently reported that the generalized stacking fault energy in Ta_2C is an order of magnitude lower for a Ta-Ta verses a Ta-C close-packed plane arrangement. This result would support that the energetically favorable shear would follow the removal of the carbon plane. For the faulted Ta_6C_5 phase to form, every sixth close packed carbon plane would be removed and sheared in sequential sequence with every five Ta-C stacks to create the unit cell; similarly, every fourth close packed carbon plane would be removed and sheared in sequential sequence with every three Ta-C stacks to create the unit cell of Ta_4C_3; and so forth. This removal and shear patterning provides qualitative insights into why the Ta_6C_5 phase (or higher ordered fault-forming phases) may not readily form as it requires longer-range vacancy ordering over multiple sequences of Ta/C layered planes.

Considering the enthalpies of formation of the structures found from the USPEX codes, it is clear there is a competition between the vacancy ordered forms of the B1 structure and those phases that are essentially formed from stacking faults. At the composition of Ta_6C_5,the faulted structures is 0.04 eV higher than the vacancy ordered structure. However, at the Ta_4C_3 composition, the faulted zeta-phase forms as described above. In examining the DFT results, it is found that the second lowest energy Ta_4C_3 structure is the C2/c vacancy ordered phase, Table II, and is indicated by its location on the 'metastable' convex hull plot by the dashed arrow in figure 2(b). This clearly indicates an energy competition present in these substoichiometric compounds between fault-forming and vacancy order rock-salt based phases, with the fault-forming structures becoming more thermodynamically favorable with further loss of carbon.

Table III. The stacking sequences of all the faulted structures in tantalum carbides. The Roman letters represent the metal close-pack stacking sequence and the Greek letters represent the equivalent for the carbon layers.

TaC	Ta_6C_5	Ta_4C_3	Ta_3C_2	Ta_2C
A	A	A	A	A
γ	γ	γ	γ	γ
B	B	B	B	B
α	Stacking fault	Stacking fault	Stacking fault	
C	A	A	A	
β	γ	γ	γ	
A	B	B	B	
γ	α	α	α	
B	C	C	C	
α	β	β	Stacking fault	
C	A	A	B	
β	γ	Stacking fault	α	
A	B	C	C	
γ	α	β	β	
B	C	A	A	
α	Stacking fault	γ	Stacking fault	
C	B	B	C	
β	α	α	β	
A	C	C		
γ	β	Stacking fault		
B	A	B		
α	γ	α		
C	B	C		
β	α	β		
A	C			
γ	β			
B	A			
α	Stacking fault			
C	C			
β	β			
A	A			
γ	γ			
B	B			
α	α			
C	C			
β	β			

The new 'metastable' convex hull construction in figure 2(b) also sheds light on prior experimental data where TaC, Ta_4C_3, and Ta_2C were all found to co-exist in a 63Ta:37C (at. %) compound, figure 1(b) [1]. The energies of each of these systems are very near each other and all are at the minimum when the kinetically constrained Ta_6C_5 vacancy ordered phase does not form. Since each of these phases are related to each other through the loss of carbon and formation of stacking faults, it becomes very difficult to distinguish between a true Ta_4C_3 phase and a rocksalt phase with a set of random stacking faults. Consequently, the decomposition of the TaC_{1-x} is not strongly driven to one particular phase. As alluded to above, the collective system is 'frustrated' in which phase to form. This idea is supported partially by experimental observations of the phase morphology near the Ta_4C_3 composition where the material is observed to be composed of very fine planar morphologies. Though these planar laths may appear thick in two-dimensional projection micrographs, figure 1(a), Morris et al. provided transmission electron tomography revealing their fine thickness and plate like structure in the plane of the carbide matrix [1]. Detailed microscopy work in Ta_2C [40] has also demonstrated that slightly carbon-rich Ta_2C will also create a series of faults whose stacking sequence agrees with the phase transformation from Ta_2C through Ta_4C_3 to TaC. The phase morphology and phase transformation pathways observed experimentally are very likely promoted by the close energetics of the Ta_2C, Ta_3C_2 and Ta_4C_3 phases revealed through the computed work here.

The evolutionary algorithm has been able to correctly identify the experimentally determined phases as well as the metastable phases. Considering the small energy differences between several of these phases, it is somewhat remarkable to consider how well the thermodynamic stability of these high-temperature materials is described by the used T=0K method. Regardless, this has provided new understanding between the thermodynamic competition of the vacancy ordered and stacking fault variations of these carbide phases that results in the complex microstructures reported.

Elastic properties

As noted in the introduction section, the tantalum carbides exhibit a range of mechanical responses. Through tailoring the phase content and microstructure, these attributes can be tuned for various loading demands. Since the production of single crystals can be arduous, if not impossible, for some of the compounds, computational calculations can provide an alternative way to probe the elastic properties of these phases. The elastic constants for each of the stable and metastable compounds have been computed, and compared where possible to either experimental and/or other computational investigations [15,43]. The tabulation of the elastic constants is found in Table IV. For cubic TaC, there are 3 nonzero independent elastic constants; for monoclinic C2/m and C2/c Ta_6C_5, there are 13; for $P3_112$ and $P\bar{3}m1$ with the trigonal symmetry, there are 7 and 6 respectively [44].

TABLE IV. Calculated elastic constants C_{ij}, the bulk modulus, shear modulus and hardness (GPa) of TaC,Ta_6C_5, Ta_4C_3, Ta_3C_2,and Ta_2C.

Compound	TaC	Ta_6C_5				Ta_4C_3		Ta_3C_2	Ta_2C
Space group	$Fm\bar{3}m$	C2/m	C2/c	$P3_112$	$R\bar{3}m$	$R\bar{3}m$	C2/c	$R\bar{3}m$	$P\bar{3}m1$
C_{11}(GPa)	737	494	497	499	585	571	504	521	479
C_{22}(GPa)		495	500				493		
C_{33}(GPa)		479	487	486	549	537	540	504	500
C_{44}(GPa)	175	173	169	206	211	179	179	164	133
C_{55}(GPa)		202	209				138		
C_{66}(GPa)		213	206				140		
C_{12}(GPa)	141	157	146	150	164	156	202	138	164
C_{13}(GPa)		177	178	179	188	169	130	192	149
C_{14}(GPa)				-27	-49	47		-44	-45
C_{15}(GPa)				27					
C_{16}(GPa)		-38	-38				-0.8		
C_{23}(GPa)		192	178				120		
C_{26}(GPa)		34	36				-0.7		
C_{36}(GPa)		5	-2				11.4		
C_{45}(GPa)		41	35				14.2		
B(GPa)	339.67	279.96	276.39	277.75	311	296	271	288	264.66
G(GPa)	216.90	175.87	178.40	179.71	200.4	187	161	167	148.08
k	0.64	0.63	0.65	0.65	0.64	0.63	0.59	0.58	0.56
H_v(GPa)	24.53	20.89	21.87	22.05	23.6	21.92	18.3	18.19	15.87

In order to easily compare the trends in hardness among the carbides, we estimated the elastic polycrystalline elastic constants using the well-known Voigt (G_V) and Reuss (G_R) elastic constants method [45,46,47] with the average shear modulus, G, defined as

$$G \equiv \frac{1}{2}(G_V + G_R)[45].$$

The "theoretical" hardness, H_V, for all the carbides was then estimated using

$$H_V = 2(k^2G)^{0.585}\text{-}3\ [48]$$

where k is Pugh's modulus ratio defined as G/B with B being the bulk modulus. The hardness of the Ta-C phase as a function of carbon content is plotted in figure 4. This is referred as "theoretical" hardness because it is based solely on the computed elastic constants and lacks any contribution of microstructure to hardness. It can be seen that all of the carbides elastically soften and the hardness monotonically decreases with decreasing carbon content.

Interestingly, one thing that that this derived hardness does not predict is the anomalous increase in hardness reported for substoichiometric compositions in tantalum, niobium, and vanadium carbides [49,50]. This increase in hardness appears near the Me_6C_5 composition; hence the elastic constants are insufficient to fully elucidate the experimental hardness behavior, a point that we demonstrate concretely in a later work [35]. These results demonstrate that the elastic constants of ordered tantalum carbides decrease continually with carbon loss, which corresponds to a decrease in covalent bonding which is demonstrated below.

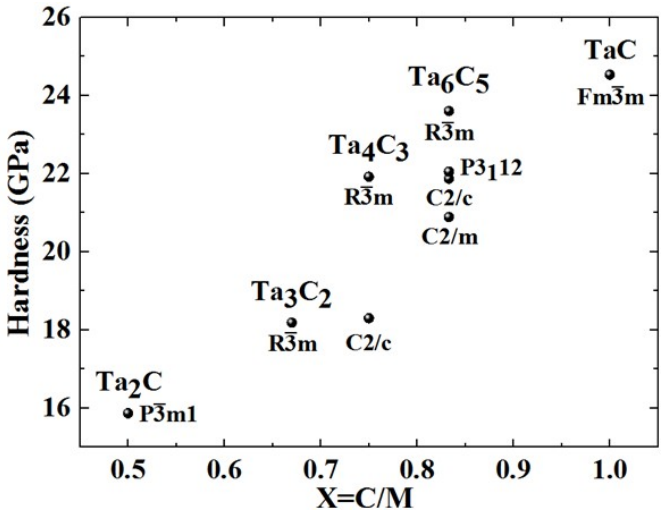

FIGURE 4. The theoretical hardness for the tantalum carbides calculated in this paper.

Electronic structure

In a prior computational study of Ta_2C [39], the bonding structure was found to be paramount in dictating the slip behavior. In this particular system, a local metallic bond was present and allowed, in specific <hkl>{hkl} orientations, an order of magnitude decreases in the generalized stacking fault energy which contributed to the enhanced plasticity. Thus, due to the correlation between bonding and properties, it is important to characterize the bonding in each of the stable tantalum carbide structures. Using the electronic DOS, the bonding characteristics in each thermodynamic stable tantalum-carbide was investigated and plotted in figure 5.

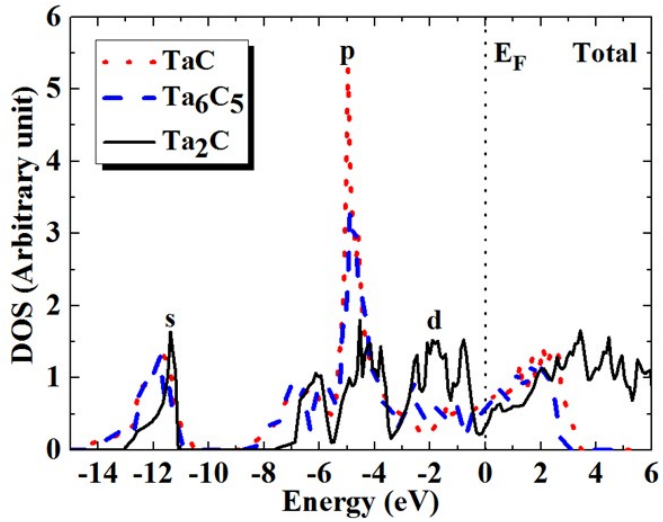

FIGURE 5. The total density of states for TaC, $Ta_6C_5$and Ta_2C_1. The DOS is normalized by the number of unit formula units in the simulation and the Fermi level has been shifted to 0 eV. (Color available on line)

The peak in the DOS for TaC is at ~ -5 eV and is associated with the *pd* bonding between the tantalum and carbon atoms, which is covalent in nature [43]. It appears that this peak decreases with carbon content, which implies it has less contribution to the bonding characteristics in the metal-rich carbides. Similarly, the density of the *d* state increases near the Fermi level, which can be interpreted as an increase in the *dd* bonding or metallic nature bonds between the tantalum atoms. This is the highest for the Ta_2C system. The change between the *p* electrons (covalent) and the *d* electrons (metallic) with carbon content results in a collective decrease in bond strength for the carbides. This corresponds to the decrease in elastic constants tabulated for the metal-rich carbides in Table III. In general, the melting temperature of a material scales with the bond strength. This trend is also evident in this plot. TaC melts at ~4200K where as Ta_2C melts at 3600K, with TaC having more of a covalent bond character. The Ta_6C_5 phase, according to Gusev [19], is lost at ~1430K, which would deviate from this trend, expect that this phase is a vacancy ordered phase and does not melt but rather becomes disordered. The computational findings appear to trend well with the physical properties of these materials.

Conclusions

By using a variable-composition *ab initio* evolutionary algorithm, we explored the stable and metastable compounds in the Ta-C system at ambient pressure and 0K. The results revealed that TaC, Ta_6C_5 and Ta_2C are the thermodynamically lowest energy configurations with Ta_4C_3 and Ta_3C_2 having slightly higher energies. The vacancy ordered form of Ta_6C_5 had three degenerate energetic structures (C2/m, C2/c, and $P3_112$). In addition, the stacking-fault based Ta_6C_5 structure has a slightly higher energy, ΔE~0.04 eV/atom than the vacancy ordered forms with an equivalent space group, $R\bar{3}m$, to the Ta_4C_3 phase. Such a small energy difference could be overcome with increasing thermal contributions, which are not considered in this computational algorithm approach. Regardless, the computational methodology provided thermodynamic stability energies that are agreement with the phases noted in these high-temperature materials. In contrast to Ta_6C_5, the Ta_4C_3 phase is commonly observed to form in experiments. By removing the kinetically constrained Ta_6C_5 phase from the convex hull plot, it was re-plotted revealing that TaC, Ta_4C_3, and Ta_2C were the lowest 'stable' phases, which are all commonly observed. The evolutional algorithm was successful at predicting all of these experimentally determined phases. Interestingly, these simulations demonstrated that in addition to the fault-formed $R\bar{3}m$ Ta_4C_3 phase, there exists a slightly higher energy, ΔE~0.01 eV/atom, vacancy ordered C2/c phase. From these computational simulations, a thermodynamic competition was noted to occur between the vacancy ordering and fault-formed phases, with the latter structures being more favorable with decreasing carbon content in TaC_{1-x}. While the stable phase predicted here are in agreement with the most comprehensive phase diagrams of Ta-C by Gusev [19], these simulations provide additional insight into the competition between the vacancy ordered B1 phases and fault forming phases that are not readily apparent from experiments.

Collectively, the close enthalpy of formation energies computed from this study for each of the stacking-fault based carbides may 'frustrate' the carbide in the co-precipitation of multiple phases in substoichiometric tantalum carbides which leads to the complex microstructures.

The DFT calculations also provided the elastic constants for each of the stable and metastable phases. As the carbon content increased, the elastic constants values increased. This has been

associated with the increase in the *pd* covalent and decrease in the metallic *dd* bonding of the carbide from the density of states.

Acknowledgments

X.X. Yu and G.B. Thompson recognize Air Force Office of Scientific Research grant FA9550-12-1-0104, Dr. Ali Sayir, Program Manager, and the University of Alabama Office for Research Post-Doctoral Fellowship Program. The USPEX code developer, Professor Artem R. Oganov and Dr. Qiang Zhu at State University of New York, Stony Brook, are also thanked for their technical assistance in the application of their code. Finally, Professor C.H. Turner of the University of Alabama and the Alabama SuperComputer (http://www.asc.edu/) is also acknowledged for access to their computational resources.

References

[1] Morris RA, Wang B, Butts D, Thompson GB. International Journal of Applied Ceramic Technology 2013;10:540.
[2] Morris RA, Wang B, Matson LE, Thompson GB. Acta Materialia 2012;60:139.
[3] Kim C, Gottstein G, Grummon D. Acta metallurgica et materialia 1994;42:2291.
[4] Wiesenberger H, Lengauer W, Ettmayer P. Acta materialia 1998;46:651.
[5] Zhang X, Hilmas GE, Fahrenholtz WG. Materials Science and Engineering: A 2009;501:37.
[6] Zhang X, Hilmas GE, Fahrenholtz WG. J Am Ceram Soc 2008;91:4129.
[7] Upadhya K, Yang J, Hoffman WP. American Ceramic Society Bulletin 1997;76:51.
[8] Wang C, Yang J, Hoffman W. Mater.Chem.Phys. 2002;74:272.
[9] Balani K, Gonzalez G, Agarwal A, Hickman R, O'Dell JS, Seal S. J Am Ceram Soc 2006;89:1419.
[10] Hackett K, Verhoef S, Cutler RA, Shetty DK. J Am Ceram Soc 2009;92:2404.
[11] Limeng L, Feng Y, Yu Z, Zhiguo Z. J Am Ceram Soc 2010;93:2945.
[12] Rudy E, Brukl C, Harmon D. V.(December 1963) 1965
[13] Rowcliffe D, Thomas G. Materials Science and Engineering 1975;18:231.
[14] Gusev AI, Rempel AA, & Magerl AJ. Disorder and order in strongly nonstoichiometric compounds: transition metal carbides, nitrides and oxides. Springer, 2001.
[15] Wu Z, Chen X, Struzhkin VV, Cohen RE. Physical Review B 2005;71:214103.
[16] Wu L, Wang Y, Yan Z, Zhang J, Xiao F, Liao B. J.Alloys Compounds 2013
[17] Wu L, Yao T, Wang Y, Zhang J, Xiao F, Liao B. J.Alloys Compounds 2012
[18] Gusev A. Journal of Experimental and Theoretical Physics 2009;109:417.
[19] Gusev A, Kurlov A, Lipatnikov V. Journal of Solid State Chemistry 2007;180:3234.
[20] Lewis M, Billingham J, Bell P. Nonstoichiometry in ceramic compounds. 1973
[21] Frisk K. ASM alloy phase diagrams centerASM International 1996
[22] Storms E. The Refractory Carbides 1967:82.
[23] Brizes W, Tobin J. J Am Ceram Soc 1967;50:115.
[24] Zaplatynsky I. J Am Ceram Soc 1966;49:109.
[25] Gusev AI. Physics-Uspekhi 2000;43:1.
[26] Oganov AR, Glass CW. J.Chem.Phys. 2006;124:244704.
[27] Lyakhov AO, Oganov AR, Stokes HT, Zhu Q. Comput.Phys.Commun. 2012
[28] Kresse G, Hafner J. Physical Review B 1993;47:558.
[29] Kresse G, Furthmüller J. Physical Review B 1996;54:11169.

[30] Tang H, Van der Ven A, Trout BL. Physical Review B 2004;70:045420.
[31] Blöchl PE. Physical Review B 1994;50:17953.
[32] Kresse G, Joubert D. Physical Review B 1999;59:1758.
[33] Perdew JP, Burke K, Ernzerhof M. Phys.Rev.Lett. 1996;77:3865.
[34] Togo A, Oba F, Tanaka I. Physical Review B 2008;78:134106.
[35] Yu X, Weinberger C, Thompson G. (under review)
[36] Hannink R, Murray M. Acta Metallurgica 1972;20:123.
[37] Hull D, & Bacon DJ. Introduction to dislocations. Butterworth-Heinemann, 2001.
[38] Laird C, Aaronson H. Acta Metallurgica 1967;15:73.
[39] Wang B, De Leon N, Weinberger CR, Thompson GB. Acta Materialia 2013;61:3914.
[40] De Leon N, Wang B, Weinberger CR, Matson LE, Thompson GB. Acta Materialia 2013
[41] Bowman AL. J.Phys.Chem. 1961;65:1596.
[42] Bowman AL, Wallace TC, Yarnell JL, Wenzel RG, Storms EK. Acta Crystallogr. 1965;19:6.
[43] Jhi S, Louie SG, Cohen ML, Ihm J. Phys.Rev.Lett. 2001;86:3348.
[44] Nye JF. Physical Properties of Cristals: Their Representation by Tensors and Matrices. Oxford University Press, 1985.
[45] Hill R. Proceedings of the Physical Society.Section A 1952;65:349.
[46] Watt JP, Peselnick L. J.Appl.Phys. 1980;51:1525.
[47] Watt JP. J.Appl.Phys. 1980;51:1520.
[48] Chen X, Niu H, Li D, Li Y. Intermetallics 2011;19:1275.
[49] Holleck H. Journal of Vacuum Science & Technology A: Vacuum, Surfaces, and Films 1986;4:2661.
[50] VINITSKY I. POROSHKOVAYA MET, JUNE 1972,--6--, 76-82 1972

Dissemination of Research Findings:

MMM 2014 – 7th International Conference on Multiscale Materials Modeling conference, Oct. 6-10th, 2014, Berkeley, CA; mmm2014berkeley.iop.org
Oral presentation:

- "Metal-rich Ceramic Phase Stability in Group IV and V Carbides and Nitrides" Xiao-Xiang Yu, Christopher R. Weinberger, Gregory B. Thompson
- "Linking Computational Stacking Fault Energies with Plasticity Mechanisms in High Temperature Carbide Ceramics" Gregory B. Thompson, Nicholas De Leon, Xiao-Xiang Yu, Billie Wang, and Christopher R. Weinberger

Poster presentation:

- "Computational Investigations into the Hardness of Metal Carbides" Xiao-Xiang Yu, Christopher R. Weinberger, Gregory B. Thompson

Materials Science and Technology (MS&T) Oct. 12-16, 2014, Pittsburg, PA matscitech.org

Oral presentation

- "Ab Initio Investigations of the Phase Stability and Hardness in Tantalum Carbides" Xiao-Xiang Yu, Christopher R. Weinberger, Gregory B. Thompson

United States Advanced Ceramics Association (USACA) January 26th – 30th, 2015, Coco Beach, FL

Oral presentation

- "Phase Stability in Tantalum Carbides and its Relationship to Microstructure and Mechanical Behavior" Xiao-Xiang Yu, Christopher R. Weinberger, and Gregory B. Thompson

The American Ceramic Society International Conference and Expo on Advanced Ceramics and Composites January 25th – 30th, 2015, Daytona, FL

Oral presentation

- "Understanding Phase Stability in the Transition Metal Group IVB and VB Carbides" Xiao-Xiang Yu, Christopher R. Weinberger, and Gregory B. Thompson

The Minerals, Metals, and Materials Society (TMS) 144th Annual Meeting & Exhbinition, March 15-19th 2015, Orlando, FL

Oral presentation

- "First-Principles Investigation on the Phase Stability in Tantalum Carbides" Xiao-Xiang Yu, Christopher R. Weinberger, and Gregory B. Thompson

Poster presentation:

- "A Non-Contact Means of Thermo-Mechanical Testing of Materials beyond 2000 °C" Chase Smith, Nicholas De Leon, and Gregory Thompson

Honors:

PI Thompson was the recipient of the 2014 Blackmon-Moody Outstanding Professor of the Year award for UA on October 24th, 2014. Below is a picture from the award ceremony. More info can be found below or with the proceeding article.

http://uanews.ua.edu/2014/10/engineering-professor-to-receive-uas-blackmon-moody-award/

Mr. Blackmon (left); President of UA, Dr. Judy Bonner (center); Professor Greg Thompson (right) receiving the award

Engineering Professor to Receive UA's Blackmon-Moody Award

TUSCALOOSA, Ala. — Dr. Gregory B. Thompson, professor of metallurgical and materials engineering at The University of Alabama, will receive the 2014 Blackmon-Moody Outstanding Professor Award at an Oct. 24 ceremony.

Since coming to the University in 2003, Thompson has received external funding from organizations such as the National Science Foundation, NASA, the Air Force Office of Scientific Research, the Office of Naval Research and the Army Research Office. These awards have totaled several millions of dollars in the support of basic and applied research in materials development.

Thompson serves as director of the Materials Science doctoral program on campus, associate director of the University's Central Analytical Facility and director of the Materials Metrology Research Consortium.

Thompson's research emphasis is in the thermodynamics and mechanisms of phase transformations and their effect on microstructure. In recent years, his research group has studied different classes of transition metal ceramics and the levels of ductility they achieve at elevated temperatures.

His research uses a variety of state-of-the-art analytical microscopes that characterize materials from the atomic to micron-length scales. He has written more than 100 peer-reviewed articles and three book chapters in his research areas of analytical microscopy and phase transformations.

Thompson has been involved in multiple outreach and service activities. In 2013 and 2014, he was a co-organizer for an ASM Materials Camp on campus, a program aimed at teaching middle- and high-school teachers how to incorporate materials engineering into secondary education classrooms.

In 2004, he co-founded the Nanoscience and Engineering High School Internship Program, a 10-week summer program in which high-school students work with UA faculty on topics like magnetic nanoparticles, sensor technology and catalysis.

In 2012, Thompson served as organizing chair for the 53rd International Field Emission Symposium that brought more than 170 scientists from 15 countries to the campus for a week-long conference on atom probe and high field nanosciences.

In 2013, Thompson was named a Crimson Tide Hometown Hero for his involvement in relief efforts following the tornado that struck Tuscaloosa April 27, 2011. Additionally, he was been recognized multiple times by the Minerals, Metals and Materials Society, having been honored as a Young Leader in 2005 and a Young Leader International Scholar in 2008.

Earning his bachelor's degree in physics from Brigham Young University in Provo, Utah, in 1996, he obtained both his master's degree and his doctorate in materials science and engineering from the Ohio State University in 1998 and 2003, respectively.

The Frederick Moody Blackmon and Sarah McCorkle Moody Outstanding Professor Award is presented annually to a UA faculty member judged to have made extraordinary research contributions that reflect credit on the individual, his or her field of study and on the University. It was created by Frederick Moody Blackmon of Montgomery to honor the memory of his grandmother, Sarah McCorkle Moody of Tuscaloosa.

The University of Alabama, a student-centered research university, is experiencing significant growth in both enrollment and academic quality. This growth, which is positively impacting the campus and the state's economy, is in keeping with UA's vision to be the university of choice for the best and brightest students. UA, the state's flagship university, is an academic community united in its commitment to enhancing the quality of life for all Alabamians.

1.

1. Report Type

Final Report

Primary Contact E-mail

Contact email if there is a problem with the report.

gthompson@eng.ua.edu

Primary Contact Phone Number

Contact phone number if there is a problem with the report

205-348-1589

Organization / Institution name

The University of Alabama

Grant/Contract Title

The full title of the funded effort.

Influence of Group IV and V Alloying Elements on the Microstructure Engineering and Deformation Behavior in Tantalum Carbides

Grant/Contract Number

AFOSR assigned control number. It must begin with "FA9550" or "F49620" or "FA2386".

FA9550-12-1-0104

Principal Investigator Name

The full name of the principal investigator on the grant or contract.

Professor Gregory Thompson

Program Manager

The AFOSR Program Manager currently assigned to the award

Dr. Ali Sayir

Reporting Period Start Date

04/01/2014

Reporting Period End Date

03/31/2015

Abstract

Transition metal carbides comprise a class of high and ultrahigh melting temperature materials with tremendous thermo-mechanical property potential. This research elucidates their phase stability and mechanical deformation mechanisms. New accomplishments in the past year includes the following:

(1) Ab initio investigations into the phase stability in Ta-C. The results revealed the most thermodynamically favorable phases (based on enthalpy of formation at 0K) are TaC, Ta6C5 and Ta2C. Interestingly, three degenerate vacancy ordered Ta6C5 structures were noted, one of which is the first ever reported. As the carbon is reduced from the stoichiometric monocarbide, the system appears to undergo a competition between precipitating vacancy-ordered and faulted-based phases, with the latter structure becoming more favorable with metal enrichment. This work provided new insights into why specific phases form and do not form within this carbide [Yu et al. Acta Materialia 80 (2014) 341]. Ongoing efforts are underway to determine the full range of phase stability in

the other group IVB, as well as group VB carbides.

(2) Building upon the computational work, the program was able to address the anomalous hardness rise noted in prior literature in the group VB carbides which is absent in group IVB carbides. This behavior is contributed to the former carbides having a lower vacancy migration energy, with NbC and VC having a near zero and negative vacancy formation energy respectively. This favorable vacancy formation and migration behavior results in the formation of Me6C5 domains. It was proposed that these domains provide “Hall-Petch” strengthening. The higher vacancy formation energy, prevalent in the group IVB carbides, likely hindered them from easily forming such phase domains which prevents the anomalous sub-stoichiometric rise in hardness. Hence, the competition between elastic constant softening and microstructure-based effects in the group VB carbides is suspected to cause the peculiar hardness peak [Yu et al J of European Ceramic Society 35 (2015) 95].

(3) The program resolved the outstanding question of why group IVB monocarbides slip on {110} planes whereas group VB carbides slip on {111} at room temperature. HfC (group IVB) and TaC (group VB) were used as the case study materials where upon Vicker’s indentation was performed. TEM dynamical diffraction quantified the slip systems with complimentary density functional theory generalized stacking fault energies (GSFEs) used to determine the predicted energy hierarchy for slip. It was found that group VB carbides can stabilize an intrinsic stacking fault (ISF) on the {111} plane that is absent in the group IVB carbides. These results debunk prior hard sphere based model interactions that have been propagated for decades to explain the slip discrepancies. This ISF allows the group VB carbides to circumvent the lower {110} GSEF surface. Also found was that TaC, regardless of GSEF surface, was lower than HfC, which was experimentally manifested as a higher dislocation density. (De Leon et al. Physical Review Letters, in press (2015).

(4) Over the past year, the program has constructed a new electrical magnetic mechanical testing apparatus that can provide a non-contact means of thermo-mechanical testing these carbides up to their melting temperature. The improvements include a larger field strength electromagnet, which will enable larger samples to be tested. In addition, a multi-point laser displacement unit for real-time creep measurements from the entire length of the bar, not just the region of maximum displacement, has been added. The testing apparatus is currently waiting on a custom chamber to house the testing equipment which will isolate the samples from the environment preventing deleterious oxidation effects at elevated temperature.

(5) Over the past year, the program has disseminated the findings through 6 contributed talks and 2 poster at various professional society meetings. The PI has been invited to give a key note lecture on the subject of carbides at the forthcoming ECI Ultrahigh Temperature Ceramics Conference in April 2015.

(6) One MS student, Chase Smith, graduated under the program who will be continuing his doctoral studies through a follow-on effort. One PhD candidate, Nicholas De Leon, passed his PhD proposal defense and is on track to defend his dissertation from the work collected under this program in fall 2015.

(6) The PI was awarded the 2014 Blackmon-Moody Outstanding Professor of the Year at The University of Alabama. This award recognizes a faculty member for their singular research accomplishments bringing credit to the capstone institution.

Distribution Statement

This is block 12 on the SF298 form.

Distribution A - Approved for Public Release

Explanation for Distribution Statement

If this is not approved for public release, please provide a short explanation. E.g., contains proprietary information.

SF298 Form

Please attach your SF298 form. A blank SF298 can be found here. Please do not password protect or secure the PDF The maximum file size for an SF298 is 50MB.

AFD-070820-035.pdf

Upload the Report Document. File must be a PDF. Please do not password protect or secure the PDF . The maximum file size for the Report Document is 50MB.

Technical findings YR 3 AFOSR_2.pdf

Upload a Report Document, if any. The maximum file size for the Report Document is 50MB.

Archival Publications (published) during reporting period:

Nicholas De Leon, Xiao-xiang Yu, Hang Yu, Christopher R. Weinberger, and Gregory B. Thompson "On How Bonding Regulates Slip Differences in the B1 Monocarbides" accepted and in press, Physical Review Letters (2015)

Xiao-Xiang Yu, Gregory B. Thompson, and Christopher R. Weinberger "Influence of carbon vacancy formation on the elastic constants and hardening mechanism in transition metal carbides" Journal of the European Ceramic Society 35 (2015) 95-103

Xiao-Xiang Yu, Christopher R. Weinberger, and Gregory B. Thompson "Ab initio investigations of the phase stability in tantalum carbides" Acta Materialia 80 (2014) 341-349

Gregory B. Thompson and Christopher R. Weinberger "Tantalum Carbides: Their Microstructures and Deformation Behavior," contributed chapter in Ultra-high Temperature Ceramics: Materials for Extreme Environment Applications, edited by W.G. Fahrenholtz, E.J. Wuchina, W.E. Lee, and Y. Zhou, Wiley (2014), ISBN: 978-1-118-70078-5

Changes in research objectives (if any):

None

Change in AFOSR Program Manager, if any:

None

Extensions granted or milestones slipped, if any:

None

AFOSR LRIR Number

LRIR Title

Reporting Period

Laboratory Task Manager

Program Officer

Research Objectives

Technical Summary

Funding Summary by Cost Category (by FY, $K)

	Starting FY	FY+1	FY+2
Salary			
Equipment/Facilities			
Supplies			
Total			

Report Document

Report Document - Text Analysis

Report Document - Text Analysis

Appendix Documents

2. Thank You

E-mail user

Mar 30, 2015 14:49:23 Success: Email Sent to: gthompson@eng.ua.edu